



Alkali metal and rare earth element evolution of rock-forming minerals from the Gatumba area pegmatites (Rwanda): Quantitative assessment of crystal-melt fractionation in the regional zonation of pegmatite groups

Niels Hulsbosch^{a,*}, Jan Hertogen^a, Stijn Dewaele^b, Luc André^b, Philippe Muchez^a

^a *Geodynamics and Geofluids Research Group, Department of Earth and Environmental Sciences, KU Leuven, Celestijnenlaan 200E, B-3001 Leuven, Belgium*

^b *Department of Geology and Mineralogy, Royal Museum for Central Africa (RMCA), Leuwensesteenweg 13, B-3080 Tervuren, Belgium*

Received 31 October 2013; accepted in revised form 4 February 2014; Available online 20 February 2014

Abstract

This study presents a general model for the evaluation of Rayleigh fractional crystallisation as the principal differentiation mechanism in the formation of regionally zoned common and rare-element pegmatites. The magmatic evolution of these systems from a granitic source is reconstructed by means of alkali element and rare earth element (REE) analyses of rock-forming minerals (feldspars, micas and tourmaline), which represent a whole sequence of regional pegmatite zonation. The Gatumba pegmatite field (Rwanda, Central Africa) is chosen as case study area because of its well-developed regional zonation sequence. The pegmatites are spatially and temporally related to peraluminous G4-granites (986 ± 10 Ma). The regional zonation is developed around a G4-granite and the proximal pegmatites grade outwardly into biotite, two-mica and muscovite pegmatites. Rare-element (Nb–Ta–Sn) pegmatites occur most distal from the granite.

Alkali metal fractionation trends in pegmatitic K-feldspar (Rb 350–6000 ppm, Cs 2–160 ppm) and muscovite (Rb 670–7000 ppm, Cs 10–150 ppm) define a single and continuous trend, which is modelled by Rayleigh fractional crystallisation, starting from a parental granite composition (G4-composition: K 3.1 wt%, Rb 222 ppm, Cs 11 ppm). The fractionation model shows, moreover, that the pegmatites adjacent to the parental pluton are the least fractionated, and the distal pegmatites are the most fractionated. Biotite pegmatites form from 0% to 69% crystallisation, two-mica pegmatites from 69% to 92%, and muscovite pegmatites from 92% crystallisation onwards. The extreme Rb- and Cs-enrichment in rare-element pegmatites requires at least 98% fractionation of the initial G4-granite composition. Mathematical derivation of the K/Rb versus Cs relationship in K-feldspars confirms Rayleigh fractional crystallisation as the main differentiation process in the development of regional pegmatite zonation. Moreover (1) it demonstrates the continuity of the fractionation process from biotite pegmatites to rare-element pegmatite and indicates a genetic link among them; and (2) it allows a general evaluation of pegmatite fields in terms of system parameters, i.e. the initial element concentration in the granitic melt and partition coefficients.

REE patterns of the rock-forming minerals (feldspars, muscovite, biotite and schorl) show a distinct transition along the regional zonation. They evolve from sloping fractionated to more flat patterns starting from the biotite up to the muscovite pegmatites. Minerals from the rare-element pegmatites (feldspars, muscovite and elbaite) show again more fractionated, heavy REE-depleted patterns. The observed evolution in the REE patterns corresponds to early crystallisation of light

* Corresponding author. Tel.: +32 16 372290; fax: +32 16 322980.
E-mail address: niels.hulsbosch@ees.kuleuven.be (N. Hulsbosch).

REE-enriched monazite and a late crystallisation of mainly cogenetic heavy REE-enriched phases such as apatite, columbite-group minerals and beryl. Modelling of Rayleigh fractionation, starting from an initial parental granite (G4-composition: La_N/Yb_N 10 and $\sum\text{REE}$ 83), shows that this evolution in mineral REE pattern is the result of fractional crystallisation of the pegmatitic melt and precipitation of REE-incorporating minerals such as monazite and apatite.

Consequently, trace element modelling indicates that Rayleigh fractional crystallisation governs the mineralogical and geochemical evolution from a granite source to common and eventually rare-element pegmatites. This mechanism shows that granitic pegmatites are extremely fractionated, residual melts which are genetically and directly connected to a main granite body.

© 2014 Elsevier Ltd. All rights reserved.

1. INTRODUCTION

Granitic pegmatites form an intrinsic, and genetically important, part of granitic intrusions in most orogenic belts (Černý, 1991a,b; Černý and Ercit, 2005; Černý et al., 2012a). They are characterised by strong enrichment in incompatible lithophile elements such as Rb, Cs, Li, Be and Sn and are often associated with Nb–Ta–Sn–W mineralisation (Simmons and Webber, 2008; Linnen et al., 2012). Granitic pegmatites have been the focus of much recent discussion, and their petrogenesis is still controversial (London, 2008; London and Morgan, 2012; Thomas et al., 2012; Thomas and Davidson, 2013). Recent investigations on granitic pegmatites have mainly focussed on rare-element pegmatite types, i.e. late stage end-members of an extremely differentiated magma, and the processes related to their internal zonation (e.g. Webster et al., 1997; Tindle and Breaks, 2000; Alfonso et al., 2003; Sirbescu and Nabelek, 2003; Kontak, 2006; Alfonso and Melgarejo, 2008; Kontak and Kyser, 2009; London, 2005a, 2014; Thomas et al., 2012). However comparatively few studies have quantitatively documented the gradual evolution of a cogenetic group of pegmatites, which is an ideal test-case to quantify the patterns of enrichment of the residual melt in incompatible rare-elements (Černý et al., 1985; Mulja et al., 1995; Selway et al., 2005). One of the problematic aspects in the evolution of these rocks pertains to the causes of regional zonation in ‘pegmatite groups’ (cf. London, 2005a; Simmons and Webber, 2008). Černý (1991a) defined the ‘pegmatite group’ as the basic genetic unit of association among individual pegmatite bodies. Differentiation seen in a group of pegmatite dikes is thought to originate from differentiation of a common source pluton, such that continuous or episodic melt extraction, coupled with continuous crystallisation, produces the regional zonation towards more fractionated, distal pegmatites (e.g. Trueman and Černý, 1982; Černý, 1991b). However, Roda-Robles et al. (1999) proposed that the regionally zoned granite-pegmatite system of the Fregeneda area was formed by three different paths of fractional crystallisation of melts generated by partial melting of quartzo-feldspathic rocks and not by differentiation from the granite.

To address these questions concerning the origin and chemical evolution responsible for regional zonation, we investigated the alkali metal (K, Rb and Cs) and rare earth element (REE) composition of rock-forming minerals

(K-feldspar, plagioclase, muscovite, biotite and tourmaline) from representative pegmatites of the well-developed regional zonation in the Gatumba area (Rwanda, Central Africa). Feldspar, mica and tourmaline are sensitive indicators of the magmatic and post-magmatic evolution of granitic pegmatites (Trueman and Černý, 1982; Černý et al., 1985; Shearer et al., 1985, 1987, 1992; Jolliff et al., 1986, 1987; Lentz, 1992; Keller et al., 1999; Larsen, 2002; Alfonso et al., 2003; Canosa et al., 2012; Černý et al., 2012a,b,c; Roda-Robles et al., 2012). In particular, their trace element composition can help to constrain the degree of differentiation of the magma and the relationships among different pegmatite types within a regionally zoned pegmatite group (e.g. Larsen, 2002). Nevertheless, the complex assemblages of minerals that are used in characterising differentiation trends in a pegmatite group can be an obstacle to unambiguously quantify the observed fractionation processes (cf. Černý et al., 1985). In addition, it is often implicitly assumed that systematic variations in trace elements (e.g. K/Rb ratios in K-feldspars) are controlled by differentiation processes, however careful quantitative analyses of the trends are often lacking. As such, we propose a quantitative research approach in order to analyse the chemical differentiation processes that caused the regional zonation in pegmatite fields. Specifically, a Rayleigh fractionation model has been set-up to calculate the compositional evolution of the residual melt during progressive crystallisation starting from a granitic composition up to the most fractionated pegmatite zones.

The Gatumba pegmatite field is a first-class area to study granite-pegmatite differentiation processes due to its striking well-developed regional zoning (Varlamoff, 1954, 1972; Dewaele et al., 2008, 2011; Melcher et al., 2008; Graupner et al., 2010; Hulsbosch et al., 2013). The Gatumba pegmatite field comprises a typical regional zonation consisting of four zones of pegmatites, of which three zones are barren, common pegmatites. These barren zones gradually evolve to the most fractionated, distal zone belonging to the rare-element class of Černý and Ercit (2005) and hosting Nb–Ta–Sn mineralisation (Varlamoff, 1972; Dewaele et al., 2011; Hulsbosch et al., 2013). This evolution from barren, common pegmatites to mineralised, rare-element pegmatites is a promising system to reconstruct this magmatic differentiation (cf. Olade, 1980).

2. GEOLOGICAL BACKGROUND

2.1. Regional setting

The Mesoproterozoic Kibara (KIB) and Karagwe-Ankole belts (KAB) are major geological features of eastern Central Africa (Tack et al., 2010). The KIB and KAB formed and evolved between pre-Mesoproterozoic domains: the Archaean-Palaeoproterozoic Congo Craton to the west and north, the Archaean Tanzania Craton to the east and the Bangweulu Block to the south. The two coeval belts are separated in the Democratic Republic of Congo (DRC) by the northwestern extension of the Palaeoproterozoic Ubende belt across Lake Tanganyika, i.e. the 2100–2025 Ma Rusizian basement (Theunissen et al., 1996). Both belts consist of Mesoproterozoic supracrustal units, mostly metasedimentary rocks with minor metavolcanic rocks, intruded by voluminous Mesoproterozoic peraluminous granitoid massifs ('S-type') and subordinate mafic bodies (Cahen et al., 1984 and references therein).

Tack et al. (2010) and Fernandez-Alonso et al. (2012) suggest that a first main granite generation in the KAB is related to a short-lived, intra-cratonic "tectono-magmatic" event at ~1375 Ma, during a time of prominent bimodal magmatism and extensional tectonics. This bimodal magmatism can be identified as (1) the mafic-ultramafic, Bushveld-type layered bodies of the Kabanga–Musongati alignment (Duchesne et al., 2004), which have been dated at 1374 ± 14 Ma (SHRIMP U–Pb; Tack et al., 2010); and (2) large volumes of peraluminous S-type granites with accompanying subordinate mafic rocks, which have been dated between 1383 ± 17 Ma and 1371 ± 7 Ma (SHRIMP U–Pb; Tack et al., 2010). The Hf-isotope systematics of zircon indicate that the ~1375 Ma S-type granites largely formed by re-melting of the ~2 Ga Rusizian basement rocks underlying the Mesoproterozoic sedimentary sequence. The emplacement depth of the S-type granites has been estimated to be at least 16 km (>4 kbar; Lehmann et al., 2013).

At the start of the Neoproterozoic era (~1000 Ma), compressional events occurred in the Irumide collisional belt of Zambia during Rodinia amalgamation (De Waele et al., 2008). The morpho-structural shaping of the KAB is interpreted to be the result of far-field effects of these compressional events, resulting in upright folds and the formation of a S2 cleavage (Tack et al., 2010; Fernandez-Alonso et al., 2012). At ~980 Ma, a second phase of peraluminous S-type granites intruded the KAB (Fig. 1B; regional bulk composition in Table 1), i.e. the so-called G4-generation in Rwanda (former terminology of Gérard and Ledent, 1970). This granite generation has been described as strongly peraluminous, equigranular, unfoliated leucogranites with muscovite and minor biotite (Gérard and Ledent, 1970; Lavreau and Liégeois, 1982; Fernandez-Alonso et al., 1986; Pohl, 1994). Major mineral phases are micas, albite and microcline; reported accessory minerals are apatite, tourmaline, ilmenite, monazite, xenotime and rare zircon (Gérard and Ledent, 1970; Pohl, 1994). Recent SHRIMP U–Pb dating of zircons showed an age of 986 ± 10 Ma for this generation (Tack et al., 2010). This

age is close to the Rb–Sr errorchron age of 976 ± 10 Ma for the G4-granites (Cahen and Ledent, 1979). The magmas are thought to be emplaced at shallower depths (≤ 4 kbar; Lehmann et al., 2013). This generation of S-type granites is interpreted as late- to post-kinetic with regard to the major deformation event. The post-kinetic relaxation of the KAB after the ~1000 Ma compressional event gave rise to the emplacement of these granites (Dewaele et al., 2011; Fernandez-Alonso et al., 2012). Hf-isotopic data of zircon, high initial $^{87}\text{Sr}/^{86}\text{Sr}$ values and the presence of older xenocryst, led Tack et al. (2010) to conclude that this second generation of S-type granites also formed by re-melting of the ~2 Ga Rusizian basement rocks, and that the addition of 'juvenile' mantle melt must have been minor. In addition, an important feature of the ~1375 Ma and ~980 Ma granite generations in the KAB is their frequent mutual occurrence in well-defined composite intrusions (Pohl, 1994).

Within the G4-granite composite intrusions and in their immediate surroundings numerous rare-element, Nb–Ta–Sn–Li–Be pegmatites and Sn–W hydrothermal quartz veins have been observed at several locations in Rwanda and in the neighbouring countries Burundi, Uganda and DRC (Varlamoff, 1972 and references therein; Pohl and Günther, 1991; Pohl, 1994; Romer and Lehmann, 1995; De Clercq et al., 2008; Dewaele et al., 2010; Pohl et al., 2013). Pegmatites in Rwanda have been dated by the Rb–Sr method on muscovite (Monteyne-Poulaert et al., 1962; Cahen, 1964): 975 ± 29 Ma at Nyabugogo (north of Kigali), 945 ± 28 Ma at Bijojo (Gatumba area), 940 ± 28 Ma at Gatumba (Gatumba area) and 955 ± 29 Ma at Rwinkwavu. Pegmatites from Burundi have been dated at 969 ± 17 Ma (Rb–Sr whole rock; Lehmann et al., 1994) and 969 ± 8 Ma (Rb–Sr muscovite; Brinckmann and Lehmann, 1983). The Rb–Sr dates most likely record the closure of the Rb–Sr system, and should be considered as lower estimates of the real formation ages. Taken together, these ages and the spatial relationship with the granites are strong arguments in favour of derivation from the second, ~980 Ma generation of granitoid magmas (e.g. Pohl, 1994).

2.2. The Gatumba pegmatite field

The Gatumba pegmatite field (± 150 km²) is a representative district for the study of pegmatite petrogenesis and mineralisation in the KAB (Dewaele et al., 2011; Hulsbosch et al., 2013). The area is located between two granitic batholiths: the Gitarama pluton to the east and the Kabaya pluton to the west. The granites have been emplaced in a regional series of lower greenschist facies Mesoproterozoic shallow-water metasediments and mafic dolerites/amphibolites (Gérard, 1965; Baudet et al., 1988). In the area, more than 130 individual pegmatite dikes have been mapped (Fig. 1C). Their dimensions are rather variable with thicknesses varying between several centimetres to 30 m and lengths ranging from tens of meters up to 2400 m (Dewaele et al., 2008). The pegmatites often intruded along sub-vertical S2 cleavage planes, which developed during folding associated with the ~1000 Ma deformation event (Dewaele et al., 2008, 2011; Fernandez-Alonso et al., 2012). Based on field data and mineralogical variations along the sequence,

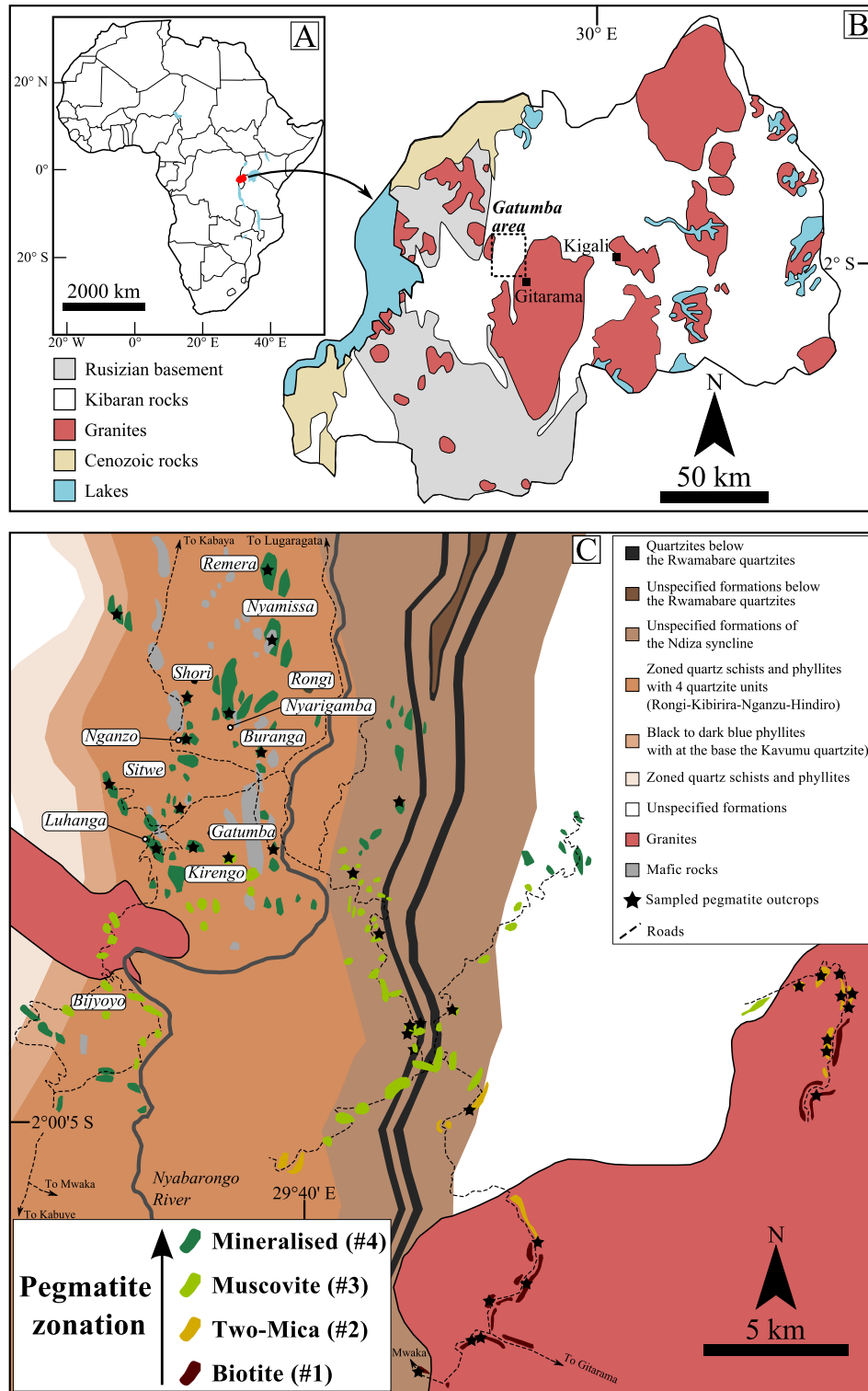


Fig. 1. (A) Geographical location of Rwanda. (B) Schematic geological map of Rwanda (after RMCA maps of Rwanda; [Fernandez-Alonso et al., 2007](#)). (C) Simplified geological map of the Gatumba pegmatite field located on the northwestern margin of the Gitarama granite (adapted from [Gérards, 1965](#); [Dewaele et al., 2011](#); [Hulsbosch et al., 2013](#)). The most important outcrops of Nb–Ta–Sn mineralised pegmatite bodies are also indicated (former Nb–Ta–Sn quarries and mining concessions).

Table 1

Major and trace element analyses of representative G4-granites (chemical data and all sample locations are according to Lehmann and Lavreau, 1988; Pohl and Günther, 1991 and references therein; the analytical data is complemented by own analyses).

Location #	Bukena 1	Kalima 10	Kirengo 3	Lutshuruk 1	Madiakala 2	Makamba 1	Mts Bia 2	Mwaka 1	Mwanza 2	Tubimbi 2
SiO ₂ (wt%)	73.1	72.4	74.1	70.2	74.1	66.3	73.7	75.4	78.8	71.2
TiO ₂	0.06	0.09	0.06	0.16	0.08	0.14	0.19	0.11	0.03	0.08
Al ₂ O ₃	14.5	15.3	14.5	16.1	14.5	18.1	13.7	14.2	12.4	15.4
Fe ₂ O ₃	0.9	1.3	1.5	2.4	1.7	2.2	1.6	0.8	0.1	1.7
MnO	0.03	0.03	0.05	0.02	0.02	0.03	0.02	0.01	0.02	0.03
MgO	0.08	0.15	0.08	0.44	0.13	0.27	0.28	0.20	0.03	0.13
CaO	0.51	0.58	0.27	0.25	0.60	1.31	0.47	0.49	1.15	0.49
Na ₂ O	3.76	3.85	4.93	2.98	3.66	4.49	1.22	3.15	3.65	2.93
K ₂ O	4.73	4.37	2.87	4.60	3.92	4.70	6.88	4.77	2.90	4.70
P ₂ O ₅	0.16	0.19	0.21	0.14	0.15	0.16	0.03	0.17	0.06	0.17
LOI	0.86	1.43	0.80	1.43	0.83	1.53	1.96	1.01	0.85	1.86
Total	98.6	99.6	99.4	98.7	99.7	99.1	100.0	100.4	100.0	98.6
A/CNK	1.2	1.3	1.2	1.6	1.3	1.2	1.3	1.3	1.1	1.4
Li (ppm)	/	278	17	130	230	230	/	/	/	15
B	/	23	12	26	5	18	/	/	/	108
F	/	1899	460	9	13	920	/	/	/	480
Zn	326	85	24	52	122	67	29	32	60	50
Rb	790	428	215	384	293	294	388	411	113	344
Sr	23	120	10	85	115	250	103	59	137	37
Y	17	7	6	10	11	7	17	13	23	10
Zr	80	42	33	36	34	32	124	58	29	46
Nb	31.4	6.6	19.3	10.0	5.0	6.0	4.2	8.8	0.1	13.5
Cs	35	37	2	17	9	13	1	8	2	6
Ba	94	199	7	251	418	383	1505	185	274	187
La	11.48	17.34	2.13	19.70	8.41	12.80	19.02	17.27	11.32	14.95
Ce	30.4	26.9	3.3	36.0	16.7	24.0	43.0	37.8	32.8	29.0
Pr	3.19	2.57	/	/	1.50	/	4.45	4.27	3.36	/
Nd	11.7	9.5	/	/	5.7	/	16.3	15.6	12.2	/
Sm	3.16	2.48	0.78	2.69	2.22	2.63	3.58	3.87	2.91	2.45
Eu	0.26	0.64	0.05	0.51	0.64	1.02	0.72	0.71	1.02	0.36
Gd	2.84	2.09	/	/	1.74	/	3.05	3.33	2.72	/
Dy	2.54	1.12	/	/	1.46	/	2.77	1.84	3.79	/
Ho	0.39	0.14	/	/	0.22	/	0.50	0.30	0.69	/
Er	1.02	0.37	/	/	0.56	/	1.45	0.84	1.98	/
Yb	0.86	0.30	0.78	0.50	0.44	0.40	1.36	0.76	1.85	1.27
Lu	0.11	0.04	0.12	0.13	0.05	0.06	0.20	0.11	0.24	0.13
Hf	2.2	1.4	1.1	1.4	1.3	1.1	3.0	1.7	0.7	1.8
Ta	18.62	1.28	1.37	1.50	0.74	1.10	0.32	1.32	0.08	2.15
W	5.8	1.5	/	/	1.7	/	2.0	2.5	1.5	/
Pb	40	38	20	26	42	40	23	32	74	52
Th	13	8	2	5	3	4	12	9	3	9
U	12	7	19	18	6	6	4	6	5	10

Coordinates: Bukena 7°40'S 27°19'E; Kalima 2°43'S 26°17'E; Kirengo 1°58'S 29°37'E; Lutshuruk 2°54'S 26°21'E; Madiakala 2°31'S 26°50'E; Makamba 2°43'S 26°16'E; Mts Bia 9°45'S 26°05'E; Mwaka 2°05'S 29°38'E; Mwanza 7°56'S 26°43'E; Tubimbi 2°47'S 28°35'E.

A/CNK = mol [Al₂O₃]/(CaO + Na₂O + K₂O).

(/ = not determined or below detection limit).

Varlamoff (1972, and references therein) proposed the differentiation sequence from G4-granite magma to barren pegmatites, to weakly zoned or unzoned Nb–Ta–Sn pegmatites.

The regional zonation sequence of the Gatumba pegmatite field has been recently redefined on the basis of textural characteristics and chemical differentiation trends (Fig. 1C; Hulsbosch et al., 2013), combined with mineral paragenesis (Dewaele et al., 2011). The zonation comprises four distinct zones which seem to have developed along the northwestern

margins of the Gitarama pluton (Fig. 1C). Barren, common pegmatites rich in schorl occur proximal in the zonation sequence. Outwardly they grade into biotite (zone #1), two-mica (zone #2) and muscovite pegmatites (zone #3). The pegmatites of zone 1 to 3 are relatively small, not mineralised and located within or close to the edges of the Gitarama granite. Nb–Ta–Sn mineralised pegmatites developed most distal in the zonation (zone #4). These most evolved pegmatites are affected by intense metasomatic-hydrothermal alteration resulting in albitisation, sericitisation and

muscovitisation (i.e. the so-called greisenisation, cf. Štemprok, 1987; Dewaele et al., 2011). Varlamoff (1954) considered the occurrence of a larger unexposed G4-granite intrusion at depth beneath the Gatumba field. Consequently, in his model the pegmatite zonation is centred on an unexposed G4-source to the southeast (Fig. 1C), close to the Gitarama granite. The Bijyoyo (Fig. 1C) and Kabaya granites would then be smaller cupolas of this larger intrusion unrelated to the source region of the pegmatites (Varlamoff, 1954).

The four pegmatite zones exhibit increasing degrees of mineralogical differentiation outward, from the Gitarama granite towards the highly differentiated pegmatite bodies located west of the Nyabarongo river (Fig. 1C). The following sequence was developed in northwestern direction starting from the Gitarama granite (see Hulsbosch et al., 2013 for a more detailed overview):

- (1) Biotite pegmatites are characterised by an equigranular assemblage of quartz, plagioclase, microcline, schorl, and biotite. Accessory garnets of the pyral-spite solid solution series are observed. The matrix is mainly composed of an anhedral, coarse-grained quartz–feldspar matrix with subhedral schorl crystals up to 4 cm in length. Microscopic textures include tartan twinned microcline, polysynthetic twinning in albite-oligoclase (An_{2-9}), perthite intergrowths in microcline, minor sericitisation of microcline, kinking of biotite cleavage, deformation twinning in feldspars as well as undulose extinction and sutured boundaries of both quartz and K-feldspar. Schorl occurs as graphic intergrowths with quartz crystals.
- (2) Two-mica pegmatites display centimetre-sized sheets of greyish muscovite macroscopically intergrown with biotite and microscopically observable as spherulitic muscovite between quartz. Quartz, blocky K-feldspars of white microcline and pink orthoclase, and albite (An_{10}) are interlocking and form the matrix. Graphic intergrowths of quartz and K-feldspar are common. The abundant large schorl crystals (~4 wt% MgO; Hulsbosch et al., 2013) display graphic intergrowths with quartz. Monazite appears as an accessory mineral enclosed in microcline, orthoclase and muscovite.
- (3) Muscovite pegmatites are mainly composed of microcline, quartz, grey-coloured muscovite, albite-oligoclase and minor blocky pink K-feldspar. Biotite is absent in these pegmatites. Schorl tourmaline is a typical constituent of the muscovite pegmatites, occurring as graphic intergrowths with quartz. Monazite is also observed and occurs enclosed by or interlocked between microcline crystals and muscovite blades.
- (4) Mineralised pegmatites are made up of pink K-feldspar (orthoclase), microcline, albite-oligoclase (An_{7-17}), quartz, Li-rich muscovite, apatite, multi-coloured and white beryl, spodumene, elbaite, columbite–tantalite, rare phosphates and other accessory phases (see e.g. Bertossa, 1965, 1967; Daltry and von Knorring, 1998 for a mineralogical overview), minor

cassiterite and secondary lepidolite after orthoclase (Varlamoff, 1963; Hulsbosch et al., 2013). Secondary albite occurs as grains with saccharoidal and cleavelandite morphologies ($An_{0.2-6.4}$). Its composition differs markedly from that of the primary magmatic plagioclase (Hulsbosch et al., 2013). The most evolved pegmatites, belonging to zone 4, are classified by Dewaele et al. (2011) as belonging to the LCT (lithium–caesium–tantalum) family according to the petrogenetic-geochemical classification of Černý and Ercit (2005). Further classification accommodates the pegmatites in the rare-element class and lithium subclass. Based on the rare-element mineralogy, the Gatumba area pegmatites include representatives of the beryl-type (beryl-columbite subtype), complex-type (spodumene subtype) and albite-spodumene type. These pegmatites have been metasomatised (25–90 vol%), causing a large part of the primary mineralogy of the pegmatites to be altered (Varlamoff, 1963). Dewaele et al. (2008, 2011) concluded, based on petrographic and stable isotope data, that the columbite-tantalite and cassiterite mineralisation mainly formed during two distinct stages: the columbite-tantalite and some of the cassiterite formed during an earlier stage of crystallisation of the pegmatites prior to the albitisation, while the major part of the cassiterite formed during the later metasomatic-hydrothermal overprint, associated with sericitisation and muscovitisation of the zone 4 pegmatites.

3. SAMPLING AND ANALYTICAL METHODS

Ideally, the determination of the bulk pegmatite composition might provide information on the magmatic evolution of the pegmatite system (e.g. Goad and Černý, 1981; Stilling et al., 2006; Černý et al., 2012b). However, this is only feasible if two conditions are fulfilled. Firstly, it must be possible to obtain reliable bulk rock analyses. Secondly, the system must have remained closed. In practice, it is difficult to acquire representative bulk samples for the Gatumba area due to the coarse grain size of most of the pegmatites and the lack of active mining. We attempted to overcome these difficulties by studying minerals separated from pegmatites. The individual pegmatite samples are fortunately rather homogeneous. They are hence representative for a given zone in the regional pegmatite evolution. Mineral specimens were separated from whole rock samples from different isolated pegmatitic bodies, i.e. from Bijyoyo, Buranga, Gatumba North and South, Gitarama-Gatumba road section, Kirengo, Luhanga, Lugaragata, Nganzo, Nyamissa, Nyarigamba, Remera, Rongi, Rugendabari, Rutobwe, Shori and Sitwe (Fig. 1C). The decimetre-sized samples have been selected from the rock and mineral collection archived at the Royal Museum for Central Africa (RMCA). The majority of these whole rock samples were collected during field campaigns conducted by Varlamoff (1954), Peeters (1956) and Gérard (1965). The exact location of the pegmatite samples is known from cartographic and archive data of the RMCA (Peeters, 1956; Varlamoff,

1956). The selected samples represent the whole succession of regional pegmatite zonation, as defined by Hulsbosch et al. (2013). Representative whole-rock, G4-granite samples (#12) have been selected from the RMCA collection for major and trace element analyses. A new set of petrographic thin sections of the samples was prepared for investigation with a polarisation microscope in transmitted light.

The granite and pegmatite samples have been subjected to similar preparatory and analytical steps. The rocks are manually broken and crushed. Pegmatite samples are further sieved to a grain size between 500 μm and 1000 μm . These grains are subsequently washed, dried at 60 °C and microscopically hand-picked with a Novax Holland stereomicroscope to obtain pure mineral fractions of feldspar, biotite, muscovite and tourmaline.

An aliquot (~1 g) of purified mineral is pulverised using a Retsch MM200 mixer mill with agate grinding tools. The powders are decomposed and dissolved by a lithium metaborate flux procedure adapted from Suhr and Ingamells (1966): 100 mg of sample and 500 mg of Spectroflux 100A LiBO_2 are fused in high-purity carbon crucibles at 1020 °C for 12 min. The redhot fusion bead is dissolved in 0.4 M HNO_3 in plastic beakers. Ultra-pure water (>18 $\text{M}\Omega\text{-cm}$) and analytical reagent grade nitric acid (prepared from subboiled 14 M HNO_3) are used for every preparatory and analytical step.

The samples have been analysed for major and minor elements with a Varian 720 ES by inductively coupled plasma–optical emission spectrometry (ICP-OES) at the

Geology Division, KU Leuven. The spectrometer is equipped with a double-pass glass cyclonic spray chamber, a concentric glass SeaSpray nebuliser, and an “extended high solids” torch. Trace elements, Rb, Cs and REE (Tb and Tm not analysed) are determined with an externally calibrated inductively coupled plasma–quadrupole mass spectrometer (ICP-QMS), type Thermo Scientific X-Series 2 with Collision Cell Technology (CCT) at the Department of Geology and Mineralogy, RMCA. Analytical precision is calculated by repeated independent sample preparation and analysis of international reference standards (BCR-1, G-2, GA, NIM-G and NIST SRM 70a). It amounts to 1–2%RSD for ICP-OES major element analysis and below 10%RSD for ICP-QMS trace element analysis. The accuracy is controlled by comparing the results obtained on the reference materials with the recommended values, and is found to be usually better than 4% for ICP-OES and below 10% for ICP-QMS. Additional G4-granite data is provided in Table 1. Geochemical data for feldspars, micas and tourmaline are given in Tables 2–4.

4. GEOCHEMICAL DATA

4.1. Alkali metals

Alkali metal ratios in K-feldspars and micas are used as monitors for pegmatite evolution. The K/Rb ratio in K-feldspars (Fig. 2A) decreases continuously from zone 1 to zone 4, with values of 216 to 158 for biotite pegmatites

Table 2

Chemical composition of representative primary magmatic feldspars from the Gatumba pegmatite zonation.

Zonation	Alkali feldspar					Plagioclase			
	Biotite	2-Mica		Muscovite	Mineralised	Biotite	2-Mica		Mineralised
		<i>Frac</i>	<i>Flat</i>				<i>Frac</i>	<i>Flat</i>	
Sample	Ga11SD50	Ga11SD60	Ga11SD62	Ga11SD47	Ga13NH01	Ga11SD57	Ga13NH37	Ga11SD65	Ga13NH38
SiO_2	64.73	62.89	66.20	66.55	63.71	65.05	66.99	64.30	63.74
Al_2O_3	18.83	18.81	19.85	18.16	18.74	20.74	20.72	20.30	20.06
CaO	0.44	0.01	0.84	0.09	0.05	1.89	1.09	1.49	1.24
Na_2O	4.51	0.50	8.07	6.28	1.96	9.86	9.52	11.67	8.80
K_2O	9.26	14.95	3.93	6.27	13.16	0.58	2.58	0.94	1.93
Rb	356	729	231	1270	6123	19	149	32	53
Cs	3	24	3	15	167	1	2	1	1
K/Rb	216	170	141	41	18	n.a.	n.a.	n.a.	n.a.
K/Cs	28,512	5223	12,131	3468	655	n.a.	n.a.	n.a.	n.a.
La	4.39	4.49	2.25	0.14	2.77	10.98	4.17	0.60	6.69
Ce	1.07	2.39	1.87	0.68	4.10	5.10	1.61	1.40	10.12
Pr	0.12	0.71	0.22	0.08	0.64	3.35	1.15	0.16	2.06
Nd	0.34	1.73	0.63	0.25	2.23	1.89	0.71	0.47	7.56
Eu	0.42	0.19	0.09	0.01	0.09	7.26	1.98	0.09	0.44
Sm	0.07	0.34	0.34	0.10	0.39	1.36	1.02	0.29	1.47
Gd	0.09	0.23	0.45	0.10	0.40	0.99	0.90	0.48	1.18
Dy	0.08	0.14	0.67	0.12	0.29	0.78	0.79	0.84	0.97
Ho	0.01	0.01	0.09	0.01	0.05	0.47	0.36	0.11	0.16
Er	0.03	0.02	0.22	0.03	0.13	0.49	0.33	0.29	0.48
Yb	0.02	0.02	0.23	0.02	0.09	0.39	0.30	0.31	0.46
Lu	b.d.	b.d.	0.04	b.d.	0.01	b.d.	0.20	0.08	0.06
La_N/Yb_N	144	147	7	5	22	28	14	1	10
Eu/Eu*	16.0	2.1	0.7	0.3	0.7	6.3	2.1	0.7	1.0

n.a. = not applicable; b.d. = below detection limits; *frac* = fractionated REE patterns; *flat* = flat REE patterns.

Table 3

Chemical composition of representative biotite and muscovite from the Gatumba pegmatite zonation.

Zonation	Biotite		Muscovite			
	Biotite	2-Mica	2-Mica		Muscovite	Mineralised
	Sample	Ga11SD56	Ga11SD62	<i>Frac</i> Ga13NH37	<i>Flat</i> Ga11SD62	Ga13NH40
SiO ₂	35.53	37.80	51.23	47.41	47.45	46.50
TiO ₂	2.26	0.46	0.05	0.06	0.05	0.03
Al ₂ O ₃	18.31	21.89	31.33	35.19	35.57	35.39
FeO (t)	21.59	19.15	1.60	2.16	1.55	2.60
MnO	0.40	0.19	0.01	0.01	0.05	<0.01
MgO	5.83	1.77	0.33	0.39	0.08	0.55
CaO	0.06	0.06	<0.01	0.01	0.06	<0.01
Na ₂ O	0.06	0.32	0.44	0.61	0.70	1.22
K ₂ O	8.96	6.53	9.35	10.45	10.14	9.62
Rb	1564	1815	807	1034	2686	3576
Cs	79	134	9	11	46	68
K/Rb	n.a.	n.a.	96	84	31	22
K/Cs	n.a.	n.a.	8995	7703	1822	1172
La	1.40	1.87	b.d.	0.70	0.09	b.d.
Ce	0.88	3.51	0.91	1.19	0.84	b.d.
Pr	0.11	0.47	0.08	0.16	0.09	0.02
Nd	0.37	1.89	0.31	0.51	0.34	0.07
Eu	0.05	0.04	0.01	0.01	0.01	0.01
Sm	0.11	1.31	0.39	0.32	0.19	0.03
Gd	0.18	2.77	1.16	0.54	0.30	0.05
Dy	0.39	4.81	2.44	0.84	0.46	0.06
Ho	0.07	0.69	0.35	0.11	0.05	0.01
Er	0.22	1.76	0.92	0.27	0.11	0.03
Yb	0.27	1.76	0.94	0.28	0.11	0.03
Lu	0.01	0.24	0.11	0.03	0.01	0.01
La _N /Yb _N	3	1	n.a.	2	1	n.a.
Eu/Eu*	1.0	0.1	0.3	0.1	0.2	0.7

n.a. = not applicable; b.d. = below detection limits; *frac* = fractionated REE patterns; *flat* = flat REE patterns.

(zone 1), 170 to 141 for two-mica pegmatites (zone 2), 41 for muscovite pegmatites (zone 3) and between 85 and 18 for mineralised pegmatites (zone 4). The K/Cs ratio of K-feldspars (Fig. 2B) decreases from ~54,000 in the less evolved pegmatites of zone 1 to ~650 in highly evolved, mineralised pegmatites.

K/Rb and K/Cs ratios in muscovite (Fig. 2C and D) exhibit a similar declining evolution from zone 1 to zone 4. The K/Rb ratios vary from 127 to 12 in muscovites along the zonation. The K/Cs ratio decreases from 8995 to 356 in muscovite. The secondary muscovites form an intrinsic part of the K/Rb and K/Cs fractionation trends and, as such, overlap with the muscovites from the mineralised pegmatites. The K/Rb and K/Cs ratios of biotites are, respectively, between 50–37 and 1100–340. The enrichment is consistent with the zonation sequence.

4.2. Rare earth elements

Representative REE patterns for the variety of pegmatite minerals, collected from all zones of the regional sequence, are presented in Figs. 3–7. Primary K-feldspar (Fig. 3) and plagioclase (Fig. 4) from biotite pegmatites have fractionated, chondrite normalised REE patterns with

heavy (H)REE-depletion ($La_N/Yb_N = 140\text{--}170$ for K-feldspar and $La_N/Yb_N = 28\text{--}245$ for primary plagioclase) and a total normalised REE budget ($\sum REE_N$) between 14–31 and 33–58, respectively. The REE patterns shift to less fractionated, more horizontal shapes starting from the two-mica pegmatites. The transition to the two-mica pegmatites is marked by the occurrence of fractionated ($La_N/Yb_N = 110\text{--}200$; $\sum REE_N = 42\text{--}114$), as well as horizontal ($La_N/Yb_N = 6$; $\sum REE_N = 29$) patterns for K-feldspar. Plagioclase crystals from two-mica pegmatites show also horizontal patterns ($La_N/Yb_N = 1.3$; $\sum REE_N = \sim 27$) as well as fractionated ones ($La_N/Yb_N = 14$; $\sum REE_N = 14$). K-feldspars of muscovite pegmatite have flat, less-fractionated patterns ($La_N/Yb_N = \pm 4$; $\sum REE_N = \pm 5$). Primary K-feldspars from the mineralised, rare-element pegmatites are defined by a total $\sum REE_N$ content between 40 and 90 and HREE-depleted patterns ($La_N/Yb_N = \sim 15$). Primary plagioclase (albite and oligoclase) from mineralised pegmatites shows similar HREE-depleted patterns ($La_N/Yb_N = \sim 20$ up to 70) with $\sum REE_N$ of 12–85. K-feldspars macroscopically related to and partially affected by albitisation, and secondary albite, with typical saccharoidal and cleavelandite morphologies, show distinctly different REE signatures compared to the primary magmatic feldspars.

Table 4
Chemical composition of representative tourmaline group minerals from the Gatumba pegmatite zonation.

Zonation Sample	Schorl			Elbaite
	Biotite Ga11SD58	2-Mica Ga11SD60	Muscovite Ga11SD49	Mineralised Ga11SD36
SiO ₂	34.30	35.86	38.48	36.73
TiO ₂	0.37	0.32	0.09	0.05
Al ₂ O ₃	31.37	34.09	31.59	37.35
FeO (t)	11.55	11.34	12.12	4.52
MnO	0.17	0.08	0.11	0.65
MgO	4.06	2.70	1.65	0.07
ZnO	0.04	0.06	0.07	0.09
CaO	0.25	0.16	0.04	0.37
Na ₂ O	2.20	1.72	1.61	2.36
K ₂ O	0.06	0.09	0.11	0.40
La	0.66	0.99	0.15	1.00
Ce	1.47	0.69	0.55	1.30
Pr	0.11	0.05	0.07	0.14
Nd	0.21	0.10	0.27	0.46
Eu	0.04	0.03	0.02	0.01
Sm	0.03	0.03	0.15	0.18
Gd	0.02	0.03	0.15	0.13
Dy	0.02	0.04	0.37	0.08
Ho	0.01	0.01	0.05	0.01
Er	0.01	0.03	0.17	0.05
Yb	0.03	0.02	0.29	0.05
Lu	0.01	b.d.	0.04	0.01
La _N /Yb _N	18	33	0.3	13.2
Eu/Eu*	5.7	2.6	0.3	0.2

b.d. = below detection limits.

Hydrothermally altered K-feldspar has a significant lower $\sum\text{REE}_N$ content varying between 3 and 20 and is marked by less-fractionated, horizontal patterns ($\text{La}_N/\text{Yb}_N = 1\text{--}9$; exceptionally 18). Secondary albite is strictly defined by overall flat REE patterns ($\text{La}_N/\text{Yb}_N = \sim 0.7\text{--}1$) and variable $\sum\text{REE}_N$.

Biotite, which is only present in biotite and two-mica pegmatites, also shows a distinct REE pattern evolution along the zonation sequence (Fig. 5). Biotite from biotite pegmatites is characterised by fractionated, HREE-depleted patterns ($\text{La}_N/\text{Yb}_N = 4\text{--}15$ and $\sum\text{REE}_N = 9\text{--}48$). Biotite from two-mica pegmatites has a more flattened pattern with a distinct light (L)REE-depletion ($\text{La}_N/\text{Yb}_N = 0\text{--}0.98$ and $\sum\text{REE}_N = 72\text{--}156$). Biotite from two-mica pegmatites shows a transition from fractionated, HREE-depleted to horizontal patterns ($\text{La}_N/\text{Yb}_N = 0.34\text{--}0.98$ and $\sum\text{REE}_N = 14\text{--}27$), as was the case for the feldspars. Moreover, LREE-segments are lower than the HREE-segments (La_N/Yb_N ratios below unity). The LREE of biotite from two-mica pegmatites are depleted compared to the same segments from biotite pegmatites and the patterns are slightly convex-upwards.

Muscovite becomes stable from the two-mica pegmatites onwards (Fig. 6). The patterns from this zone show a transition marked by the occurrence of fractionated ($\text{La}_N/\text{Yb}_N = 11$), as well as horizontal ($\text{La}_N/\text{Yb}_N \sim 1$) patterns. The LREE-segments plot lower than the HREE-segments ($\text{La}_N/\text{Yb}_N < 1$). A similar transition is observed for muscovite

from the two-mica zone compared to the other minerals: the LREE are progressively depleted but the HREE-segments stay parallel. Muscovite from muscovite pegmatites shows (1) flat to convex-up, MREE-enriched and (2) HREE-depleted patterns. Primary muscovite from rare-element pegmatites has flat patterns with minor HREE-depletion with the exception of one sample showing a fractionated pattern.

Tourmaline has been identified as schorl as well as elbaite. Schorl forms part of the biotite, two-mica and muscovite pegmatites while elbaite is restricted to the cores of mineralised pegmatites. Schorl (Fig. 7A) from biotite pegmatites shows typical HREE-depleted patterns (La_N/Yb_N ratios between 20 and 240). Schorl from two-mica pegmatites shows identical features in terms of the REE as schorl from the biotite pegmatites (La_N/Yb_N ratios of 30). Schorl from muscovite pegmatites shows a transition to flat, non-fractionated patterns with La_N/Yb_N ratios of 0.3. Primary tourmaline in mineralised pegmatites is marked by the stabilisation of elbaite (Fig. 7B).

Almost all the analysed samples have distinct Eu-anomalies, which result from the partial reduction of trivalent Eu^{3+} to divalent Eu^{2+} in magmatic conditions. The extent of the Eu-anomaly is expressed by the ratio of the observed normalised europium content (Eu), divided by the content (Eu^*) expected from interpolation of the concentrations of the neighbouring, exclusively trivalent REE. K-feldspar and plagioclase in biotite pegmatites have a distinct positive Eu-anomaly ($\text{Eu}/\text{Eu}^* = 16\text{--}45$ for K-feldspar and $\text{Eu}/\text{Eu}^* = 16\text{--}45$ for plagioclase). K-feldspar and plagioclase from the two-mica pegmatites and with fractionated patterns are also marked by positive Eu-anomalies ($\text{Eu}/\text{Eu}^* = 2\text{--}4$ and $\text{Eu}/\text{Eu}^* = 2$) whereas feldspars with horizontal patterns show weak negative anomalies ($\text{Eu}/\text{Eu}^* = 0.7$ and $\text{Eu}/\text{Eu}^* = 0.7$). K-feldspar from muscovite pegmatites developed a negative Eu-anomaly ($\text{Eu}/\text{Eu}^* = 0.3$). Feldspars from mineralised pegmatites show weakly developed negative/positive to absent Eu-anomalies ($\text{Eu}/\text{Eu}^* = 0.6\text{--}1.7$ for K-feldspar and $0.4\text{--}1.6$ for plagioclase). Biotite from biotite pegmatites has no distinct Eu-anomaly ($\text{Eu}/\text{Eu}^* = 0.92\text{--}0.99$), but the anomaly in biotite evolves to distinctly negative ($\text{Eu}/\text{Eu}^* = 0.07$) in two-mica pegmatites. The Eu-anomaly in muscovite shows the same trends as for the other minerals, i.e. for the two-mica zone more flat patterns are related to positive Eu-anomalies ($\text{Eu}/\text{Eu}^* = 2.6$) and LREE-depleted patterns with negative anomalies ($\text{Eu}/\text{Eu}^* = 0.05\text{--}0.4$). Muscovite from the muscovite zone developed a negative to absent Eu-anomaly. Muscovite from mineralised pegmatites shows similar weak negative/positive to absent Eu-anomalies ($\text{Eu}/\text{Eu}^* = 0.7\text{--}1.3$). The Eu-anomaly in tourmaline evolves characteristically from positive in schorl from biotite and two-mica pegmatites ($\text{Eu}/\text{Eu}^* = 3\text{--}5$) to negative in schorl from muscovite pegmatites and elbaite from mineralised pegmatites ($\text{Eu}/\text{Eu}^* = 0.2\text{--}0.3$). These observations suggest that the Eu-anomalies of the studied rock-forming minerals developed along the zonation from positive in Eu^{2+} -compatible minerals and absent in Eu^{2+} -incompatible minerals of the biotite pegmatites, to absent or slightly negative in the Eu^{2+} -compatible phases and negative in

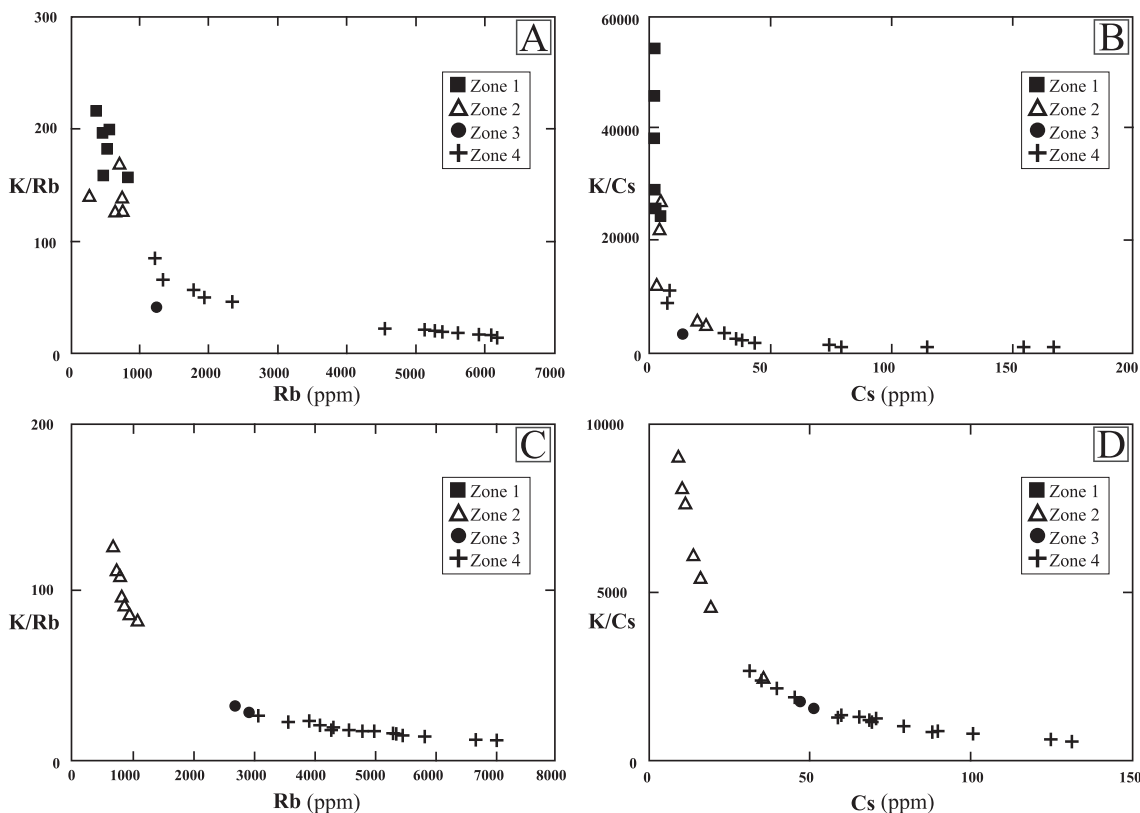


Fig. 2. K/Rb versus Rb and K/Cs versus Cs plots (cf. Černý et al., 1981, 1985) of K-feldspars (A and B) and muscovites (C and D) along the zonation sequence (zone 1 = biotite pegmatites, zone 2 = two-mica pegmatites, zone 3 = muscovite pegmatites and zone 4 = mineralised pegmatites; and ratios expressed in ppm/ppm).

Eu²⁺-incompatible phases of two-mica, muscovite and rare-element pegmatites.

5. THE FRACTIONAL CRYSTALLISATION MODEL

5.1. Evidence for Rayleigh-type fractional crystallisation

Element ratios utilising alkali earths are used prominently in petrochemical modelling of granitic compositions (Taylor, 1965; Shaw, 1968). Černý et al. (1981) focussed as one of the first on the variations in the K/Rb ratio and later on variations in K/Cs in K-feldspar as a monitor for pegmatite fractionation and as a correlation index between cogenetic groups of pegmatites (e.g. Černý et al., 1985). The approach has later been broadened to include other minerals (e.g. muscovite: Jolliff et al., 1987, 1992; Canosa et al., 2012; biotite: Lentz, 1992; Hulsbosch et al., 2013) in order to additionally constrain the degree of compositional evolution of a pegmatite system.

It is often implicitly assumed that the enrichment of Rb and Cs over K is due to fractional crystallisation, because the crystal/melt partition coefficients of K-feldspar, muscovite and biotite decrease systematically with increasing ionic radius from K⁺, over Rb⁺ to Cs⁺. Residual melts would become enriched in Rb and Cs. The lower K/Rb, K/Cs ratios and higher Rb and Cs contents of evolved bulk pegmatites

and their constituent minerals (see Fig. 2) would then be inherited from the evolved residual melts. It is also tempting to attribute the near exponential decline of the K/Rb and K/Cs ratios as shown in Fig. 2 to a ‘power-law’-type of process such as Rayleigh fractionation. However, one may not a priori rule out the possibility that other processes such as fluid fractionation caused the enrichment of Rb and Cs over K. As shown in the next paragraphs, a careful quantitative analysis of the trends of the alkali elements nonetheless provides compelling evidence for Rayleigh-type fractionation of granitic melts being the main process responsible for the enrichment of Rb and Cs in the Gatumba pegmatite field. However, there are some limitations and prerequisites associated with the use of the Rayleigh fractionation law for geological systems (see Irber, 1999 for a critical review on the applicability of the Rayleigh fractionation model). The Rayleigh (1896) fractionation law is only realistically applicable to geological systems if it can be generalised to allow the effect of changing mineral proportions and partition coefficients (Greenland, 1970). This condition can be practically fulfilled by use of quantitative ‘finite-step’ modelling, permitting to change the mineral proportions and/or partition coefficients in each discrete calculation step (e.g. applied for partial melting in Hertogen and Gijbels, 1976; see also Section 5.2.1.). However, the variation of partition coefficients with physicochemical conditions is unknown for most geological systems (Pan, 1997).

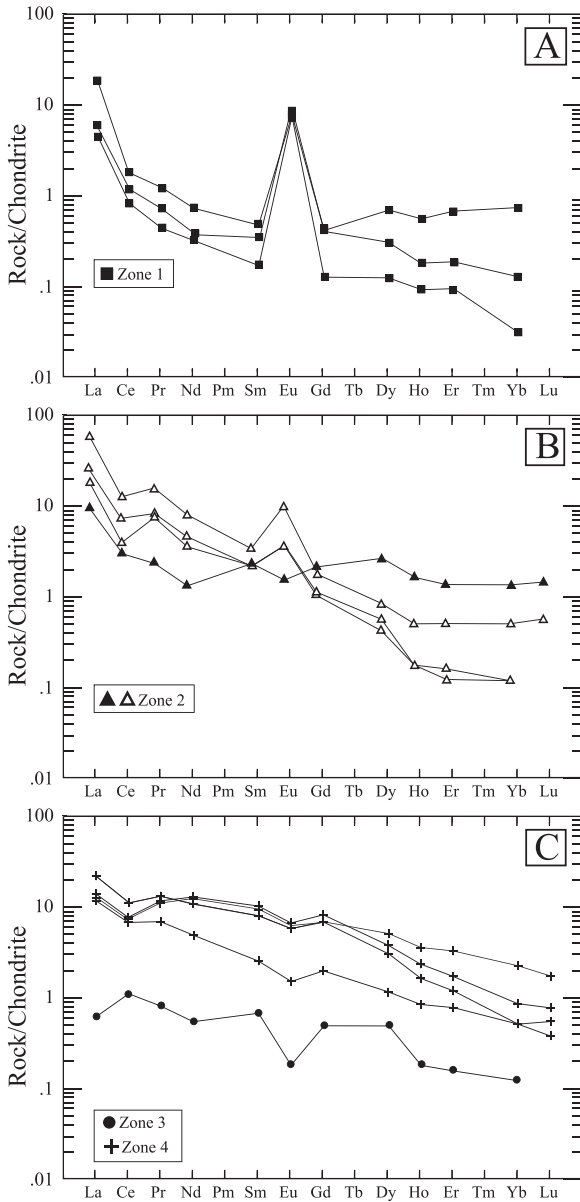


Fig. 3. Distribution of REE in primary K-feldspar along the Gatumba pegmatite zonation. A distinction has been made between the fractionated (filled triangles) and flat (open triangles) REE patterns of the two-mica pegmatite zone (zone 1 = biotite pegmatites, zone 2 = two-mica pegmatites, zone 3 = muscovite pegmatites and zone 4 = mineralised pegmatites).

The mathematical functions that describe the alkali element variation trends in linear or logarithmic form (K/Rb versus Rb ; K/Cs versus Cs , K/Rb versus Cs , etc.) in minerals from pegmatites are derived from the basic Rayleigh fractionation law:

$$\frac{C_i^{Liq}}{C_{0,i}^{Liq}} = (1 - F)^{(D_i - 1)} \quad (1)$$

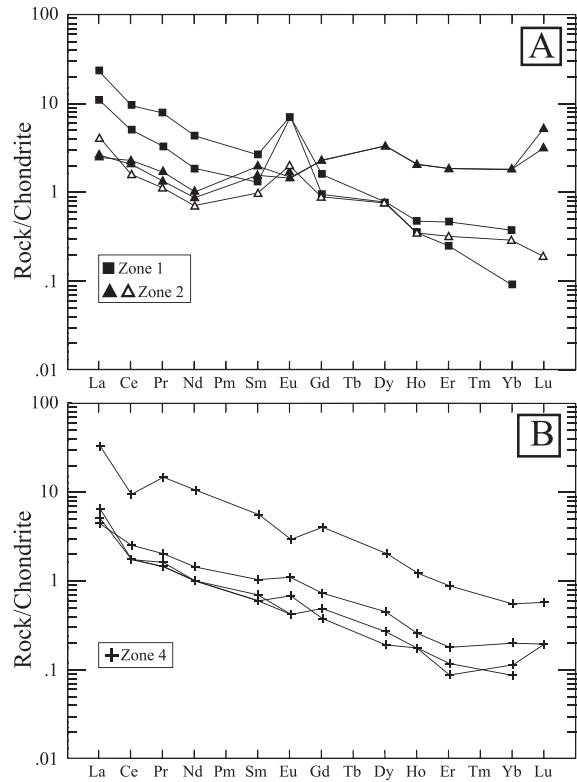


Fig. 4. Distribution of REE in primary plagioclase along the Gatumba pegmatite zonation. A distinction has been made between the fractionated (filled triangles) and flat (open triangles) REE patterns of the two-mica pegmatite zone (zone 1 = biotite pegmatites, zone 2 = two-mica pegmatites, zone 3 = muscovite pegmatites and zone 4 = mineralised pegmatites).

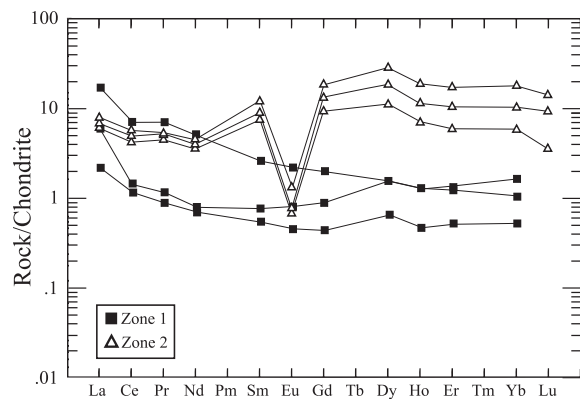


Fig. 5. Distribution of REE in biotite along the Gatumba pegmatite zonation. Biotite is only occurring in biotite and two-mica pegmatites (zone 1 = biotite pegmatites, zone 2 = two-mica pegmatites, zone 3 = muscovite pegmatites and zone 4 = mineralised pegmatites).

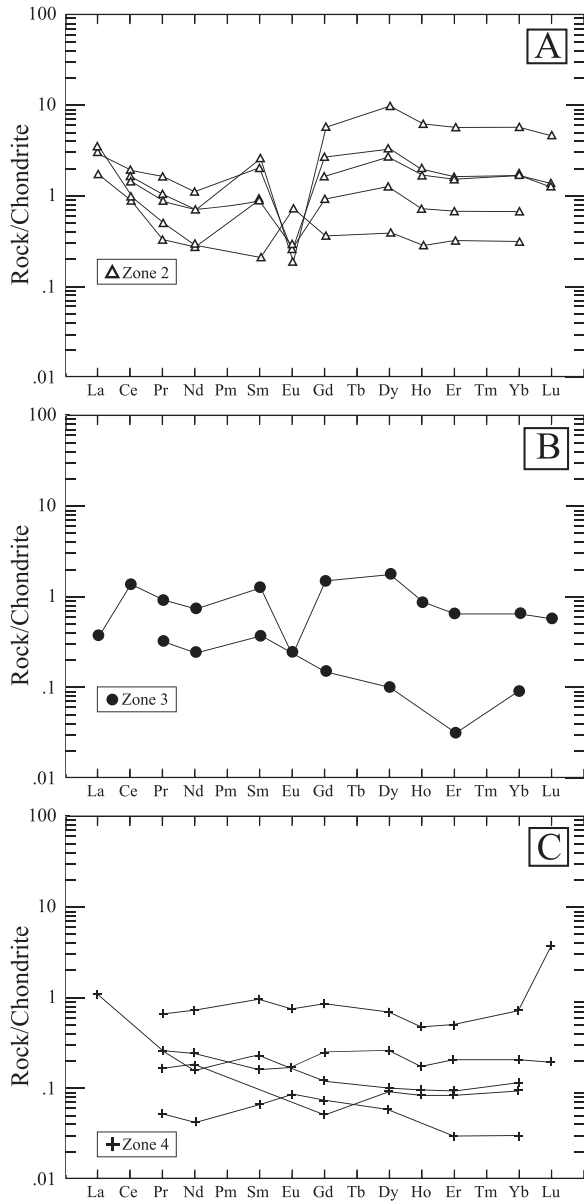


Fig. 6. Distribution of REE in muscovite along the Gatumba pegmatite zonation. Muscovite is not occurring in biotite pegmatites (zone 2 = two-mica pegmatites, zone 3 = muscovite pegmatites and zone 4 = mineralised pegmatites).

with $C_{0,i}^{Liq}$ = initial concentration of element i in the parental melt
 C_i^{Liq} = concentration of element i in the residual melt
 F = extent of crystallisation ($0 < F < 1$)
 D_i = bulk distribution coefficient of element i
 $D_i = \sum_j X_j K_{d,ij}$
 X_j = mass fraction of mineral j in the crystallising assemblage
 $\sum_j X_j = 1$
 $K_{d,ij} = \frac{C_{ij}^{Sol}}{C_i^{Liq}}$ = crystal/melt partition coefficient of element i for mineral j

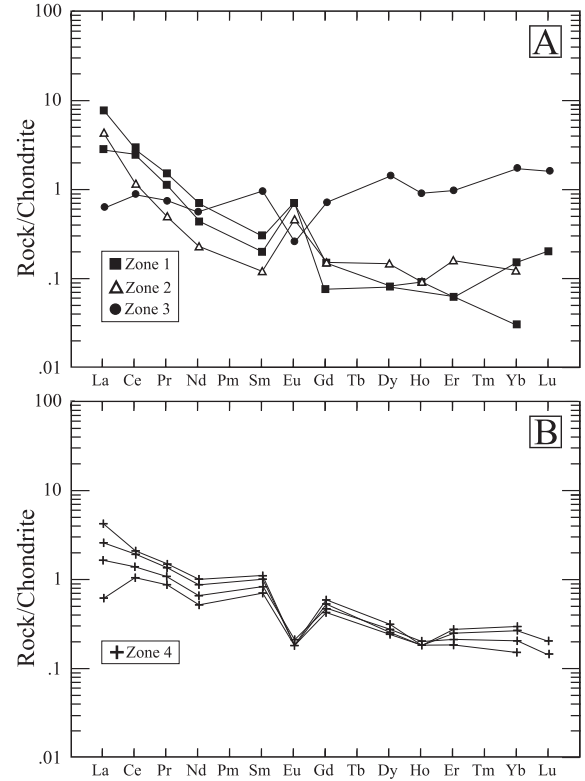


Fig. 7. Distribution of REE in tourmaline along the Gatumba pegmatite zonation.(A) schorl solid solution in biotite, two-mica and muscovite pegmatites and (B) elbaite in mineralised pegmatites (zone 1 = biotite pegmatites, zone 2 = two-mica pegmatites, zone 3 = muscovite pegmatites and zone 4 = mineralised pegmatites).

The concentration of element i in mineral j as a function of the extent F of crystallisation is then:

$$C_{ij}^{Sol} = K_{d,ij} C_{0,i}^{Liq} (1 - F)^{(D_i - 1)} \quad (2)$$

or rewritten in logarithmic form:

$$\log(C_{ij}^{Sol}) - \log(C_{0,i}^{Liq}) = \log(K_{d,ij}) + (D_i - 1) \cdot \log(1 - F) \quad (3)$$

The mathematical function describing the expected geochemical trend for a given mineral j in a three-element logarithmic graph $\log(E1/E2)$ versus $\log(E3)$ (e.g. $\log(K/Rb)$ versus $\log(Cs)$) follows from a combination of equations such as Eq. (3) for the three elements $i = 1$, $i = 2$ and $i = 3$. The equations for E1 and E2 are subtracted from each other to form a new equation from which the term $\log(1 - F)$ is eliminated using the equation for E3. The general form is:

$$\log\left(\frac{C_{1,j}^{Sol}}{C_{2,j}^{Sol}}\right) = A \cdot \log(C_{3,j}^{Sol}) + \left[\log\left(\frac{C_{0,1}^{Liq} \cdot K_{d,1,j}}{C_{0,2}^{Liq} \cdot K_{d,2,j}}\right) - A \cdot \log(C_{0,3}^{Liq} \cdot K_{d,3,j}) \right] \quad (4)$$

Table 5

Parameters applied in the alkali metal and REE Rayleigh fractionation modelling: the initial melt composition (C_0^{Liq}), mineral mass fractions for each pegmatite zonation (X_j) and representative partition coefficients (K_d). The initial melt composition is represented by an averaged, regional G-4 granite composition derived from 10 bulk rock analyses archived in the RMCA collection. Partition data in italics are interpolated or assumed based on literature data.

Alkali metals		Qz	Pl	Zrn	Afs	Mnz	Ap	Bt	Ms	Tur
Zone		X_j (%)								
Biotite		22	38	0	17.1	0	0	16.7	0	6.2
2-Mica		22	38	0	17.1	0	0	8.35	8.35	6.2
Muscovite		22	38	0	17.1	0	0	0	16.7	6.2
Mineralised		22	38	0	17.1	0	0	0	16.7	6.2
Element	C_0^{Liq}	K_d								
K	3.1 wt%	0.013	0.1	n.a.	3.12	n.a.	n.a.	2.5	2.5	0.19
Rb	222 ppm	0.014	0.09	n.a.	0.9	n.a.	n.a.	2.0	1.75	0.3
Cs	11 ppm	0.022	0.12	n.a.	0.03	n.a.	n.a.	0.27	0.16	0.056
REE		Qz	Pl	Zrn	Afs	Mnz	Ap	Bt	Ms	Tur
Zone		X_j (%)								
Biotite		22	37.9	0.1	17.1	0	0	16.7	0	6.2
2-Mica		22	37.9	0.1	17.1	0.1	0	8.35	8.35	6.1
Muscovite		22	37.9	0.1	17.1	0.1	0	0	16.7	6.1
Mineralised		22	37.9	0.1	17.1	0	0.1	0	16.7	6.1
Element	C_0^{Liq}	K_d								
La	12 ppm	0.01	0.2	1.3	0.08	3200	456	0.08	<i>0.003</i>	<i>0.08</i>
Ce	26 ppm	0.01	0.14	2.04	0.022	3412	569	0.062	<i>0.01</i>	<i>0.05</i>
Pr	4 ppm	<i>0.01</i>	<i>0.12</i>	<i>2.54</i>	<i>0.014</i>	3569	764	0.05	<i>0.006</i>	<i>0.031</i>
Nd	14.7 ppm	0.01	0.12	3.35	0.02	3726	855	0.058	<i>0.0045</i>	<i>0.02</i>
Sm	3.5 ppm	0.01	0.12	3.79	0.02	2859	1105	0.065	<i>0.0028</i>	<i>0.01</i>
Eu	0.4 ppm	0.04	1.2	0.45	1.2	228	23.8	0.1	<i>0.03</i>	<i>0.1</i>
Gd	3.1 ppm	<i>0.01</i>	0.1	9.21	<i>0.01</i>	2144	2133	0.095	<i>0.0055</i>	<i>0.01</i>
Dy	2.7 ppm	0.01	0.1	38.8	0.02	1429	2750	0.13	<i>0.0065</i>	<i>0.014</i>
Ho	0.5 ppm	<i>0.01</i>	<i>0.065</i>	74.5	<i>0.02</i>	920	3143	0.18	<i>0.0068</i>	<i>0.018</i>
Er	1.3 ppm	<i>0.01</i>	<i>0.05</i>	165	<i>0.022</i>	595	3250	0.19	<i>0.0055</i>	<i>0.018</i>
Yb	1.1 ppm	0.01	0.05	278	0.015	273	2810	0.21	<i>0.0075</i>	<i>0.012</i>
Lu	0.1 ppm	0.01	0.065	923	0.02	174	2981	0.2	<i>0.009</i>	<i>0.02</i>

References: (Qz) Nash and Crecraft (1985), (Pl) Philpotts and Schnetzler (1970), Nash and Crecraft (1985), Bea et al. (1994a); (Zrn) Bea et al. (1994a); (Afs) Long (1978), Nash and Crecraft (1985), Icenhower and London (1996), London (2005b); (Mnz) Yurimoto et al. (1990); (Ap) Bea et al. (1994a); (Bt) Philpotts and Schnetzler (1970), Nash and Crecraft (1985), Icenhower and London (1995), London (2005b); (Ms) Philpotts and Schnetzler (1970), Icenhower and London (1995) London (2005b), Adam and Green (2006); (Tur) van Hinsberg (2011). n.a. = not applicable.

and has the form: $y = A \cdot x + B$. The slope of this linear relationship is:

$$A = \frac{(D_1 - D_2)}{(D_3 - 1)} \quad (5)$$

and the intercept with the y-axis:

$$B = \log \left(\frac{C_{0,1}^{Liq} \cdot K_{d,1,j}}{C_{0,2}^{Liq} \cdot K_{d,2,j}} \right) - A \cdot \log(C_{0,3}^{Liq} \cdot K_{d,3,j}) \quad (6)$$

Hence, in an ideal Rayleigh fractional crystallisation sequence of a given melt (cf. Hanson, 1978), the concentrations of three elements in a given mineral plotted in a $\log(E1/E2)$ versus $\log(E3)$ graph should meet three requirements: (1) the data define a linear array; (2) the slope of the trendline depends on the values of the bulk distribution coefficients; (3) the intercept value is determined by the bulk distribution coefficients, the partition coefficients and the

initial concentrations of the elements in the parental melt. It is assumed here that the values of the partition coefficients and the bulk distribution coefficients do not change substantially over the crystallisation interval.

A very compelling argument in favour of Rayleigh-type fractional crystallisation could be made if the data would indeed comply with the three requirements above. This will be checked for the case of the Gatumba pegmatites below. A first test involves the two elements K and Rb (relationship K/Rb versus Rb) in the K-feldspar minerals. A two-element graph is a simplified case of Eq. (4), as element 2 is identical to element 3. For a $\log(K/Rb)$ versus $\log(Rb)$ the equation is (omitting the subscript for the mineral):

$$\log \left(\frac{C_K^{Sol}}{C_{Rb}^{Sol}} \right) = A \cdot \log(C_{Rb}^{Sol}) + \left[\log \left(C_{0,K}^{Liq} \cdot K_{d,K} \right) - (1 + A) \cdot \log \left(C_{0,Rb}^{Liq} \cdot K_{d,Rb} \right) \right] \quad (7)$$

with

$$A = \frac{(D_K - D_{Rb})}{(D_{Rb} - 1)} \quad (8)$$

A peculiar aspect of modelling trends such as (K/Rb) versus Rb originates from the observation that geochemical variation trends of granitic systems generally show rather constant K_2O contents (e.g. Taylor, 1965). In terms of Rayleigh fractionation this implies that the bulk distribution coefficient of potassium remains close to unity over a broad range of fractionation. This is actually to be expected, because the bulk distribution coefficient is a weighted average of a high potassium K_d for K-feldspar (ca. 3) and the low K_d 's for other minerals (mainly quartz and plagioclase). If it is assumed that D_K is near to unity, then the parameter A in Eqs. (7) and (8) reduces to -1 , and the expression for the log(K/Rb) versus Rb trend becomes:

$$\log\left(\frac{C_K^{Sol}}{C_{Rb}^{Sol}}\right) = -\log(C_{Rb}^{Sol}) + \log(C_{0,K}^{Liq} \cdot K_{d,K}) \quad (9)$$

The slope is expected to be close to -1 , and the intercept equal to $\log(C_{0,K}^{Liq} \cdot K_{d,K})$. An analogue expression for a (K/Rb) versus Rb graph is:

$$\left(\frac{C_K^{Sol}}{C_{Rb}^{Sol}}\right) = (C_{0,K}^{Liq} \cdot K_{d,K}) \frac{1}{C_{Rb}^{Sol}} \quad (10)$$

This (Eq. (10)) is the equation of a hyperbola, with the x - and y -axes of the graph as asymptotes (cf. Fig. 2). But a caveat is in order here. One could argue that any fractionation process that kept the potassium content more or less constant and enriched Rb relative to K would produce a hyperbola in a linear graph. This is indeed true. However, it would be a complete coincidence if this process would produce an intercept in a log(K/Rb) versus log(Rb) plot that would be consistent with the numerical value of the product $(C_{0,K}^{Liq} \cdot K_{d,K})$. In the particular case of log(K/Rb) versus log(Rb) or log(K/Cs) versus log(Cs), the value of the intercept is the crucial test parameter. For the Gatumba pegmatite K and Rb data for 21 K-feldspar samples (omitting the two samples that plot off the main trend in Fig. 2) define a very good linear trend in a log(K/Rb) versus log(Rb) graph ($R^2 = 0.991$). The slope of the line is equal to -0.92 , the intercept equal to 4.74. The theoretically expected intercept is equal to 4.96 for an estimated K content of 3.1 wt% K in the initial granitic magma, and a reasonable value of 3 for the potassium K_d for K-feldspar. The good correspondence between observed and theoretical values is evidence in favour of a Rayleigh-type fractionation process.

A second, more complex test involves the three-element relationship log(K/Rb) versus log(Cs), shown in Fig. 8. The theoretical function for Rayleigh fractionation is (omitting again the subscript for the mineral):

$$\log\left(\frac{C_K^{Sol}}{C_{Rb}^{Sol}}\right) = A \cdot \log(C_{Cs}^{Sol}) + \left[\log\left(\frac{C_{0,K}^{Liq} \cdot K_{d,K}}{C_{0,Rb}^{Liq} \cdot K_{d,Rb}}\right) - A \cdot \log(C_{0,Cs}^{Liq} \cdot K_{d,Cs}) \right] \quad (11)$$

with

$$A = \frac{(D_K - D_{Rb})}{(D_{Cs} - 1)} \quad (12)$$

A linear fit through 23 data for K-feldspar ($R^2 = 0.881$) yields a slope of -0.57 and an intercept value of 2.42. The expected value of the intercept is equal to 2.63 for the following estimates of the system parameters: initial concentrations in the granitic melt of 3.1 wt% K, 220 ppm Rb, 10 ppm Cs; K-feldspar partition coefficients of 3, 0.8 and 0.15 for K, Rb and Cs, respectively. The correspondence between the two values is certainly good, and warrants a further quantitative elaboration of the Rayleigh fractionation model in the next sections.

5.2. Quantitative assessment of fractional crystallisation

5.2.1. Alkali metal fractionation model

The treatment above (Section 5.1.) examined if the geochemical variation in Gatumba pegmatite minerals is to a reasonable extent consistent with Rayleigh fractionation. However, this yielded little insight into the degree of crystallisation of the initial granitic magma required to produce the pegmatites. In terms of ore genesis this is nonetheless a very important parameter. The quantitative 'forward model' presented below is based on estimates of the initial concentrations of the alkali elements in the assumed initial G4-granitic magma. Further necessary input data are estimates of the mass fractions of crystallising minerals, and values of the partition coefficients. The latter have been culled from the literature. The input data are summarised in Table 5. The residual melt evolution with protracted differentiation will subsequently be calculated based on "finite step" numerical simulation of Rayleigh's law.

The fractionation modelling of the alkali elements has accordingly two main objectives: (1) quantitative evaluation of Rayleigh fractional crystallisation as the main differentiation process responsible for the regional pegmatite zonation in Gatumba, and (2) geochemical assessment of the G4-granite generation as the parental magma for the Gatumba pegmatite field (i.e. syngenetic granite-pegmatite system). The model incorporates the mineralogical evolution along the regional zonation sequence and hence its achievability is mainly enhanced by the relatively uncomplicated bulk mineralogy of the three proximal pegmatite zones (i.e. biotite, two-mica and muscovite zones) which tend to show granitic mineral modes. However the most distal pegmatite zone, i.e. the mineralised pegmatites, shows strongly deviating mineral modes with high enrichment in lithium-rich and phosphate minerals. Consequently the main target of the model is to constrain petrochemically the derivation of the biotite, two-mica and muscovite pegmatites from its inferred plutonic G4-granite parent and to end-up with a representative composition for the mineralised pegmatite zone.

The model is in general based on the crystal/melt partition coefficient (K_d) and bulk distribution coefficient (D) (Fig. 9). Both coefficients are used as input in the equation of Rayleigh for fractional crystallisation together with the concentration of the trace element in the parental melt before any crystallisation has occurred (C_0^{Liq}). The degree of

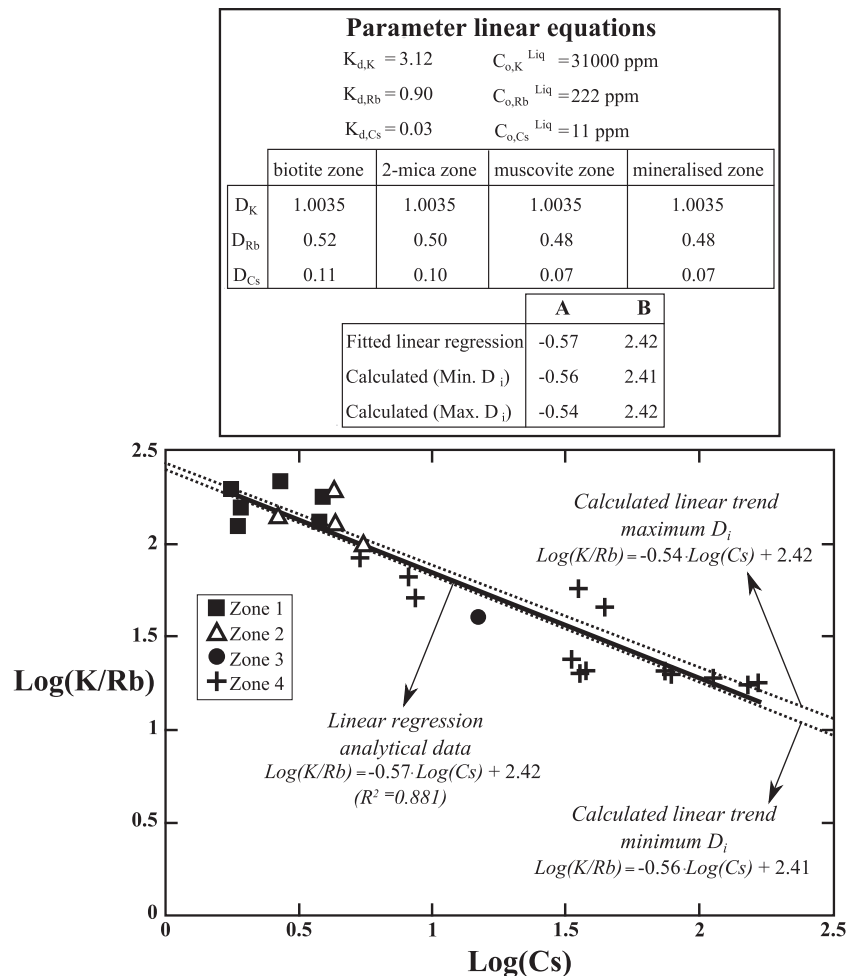


Fig. 8. K/Rb versus Cs relationship in K-feldspars sampled along the regional Gatumba pegmatite zonation. The linearity of the logarithmic transformed analytical data is consistent with the process of fractional crystallisation (see Section 5.2.). The regression line equation fitted through the data points ($R^2 = 0.881$) is defined by a slope (A) of -0.57 and y -intercept (B) of 2.42 . Theoretical derivation of the linear relationship is according to Eqs. (11) and (12) and is based on the representative set of petrogenetic parameters used in the Rayleigh fractionation model. These parameters are system-dependent and characteristic for the Gatumba pegmatite field: the alkali metal partition coefficients (K_d), initial concentrations in the parental melt ($C_{o,i}^{Liq}$) and calculated bulk distribution coefficients (D). Due to the minor variations in D for Rb and Cs along the pegmatite zonation, minimal and maximal values can be obtained for the calculated slopes (-0.56 and -0.54) and y -intercepts (2.41 and 2.42). Both calculated trends demonstrate a high-degree of overlap with the analytically defined regression trend, demonstrating the petrogenetic appropriateness of the applied model parameters and the consistency of the fractionation model itself.

fractionation (F) is modelled as a variable. The intended trace element concentration in the mineral of interest (C^{Sol}) is recalculated from the element concentration in the residual melt by use of the partition coefficient.

Specifically, the alkali metal variations in K-feldspar and muscovite along the zonation sequence are applied to constrain the total degree of fractionation of the entire pegmatite system, as well as the degree of fractionation between the different pegmatite zones. Due to the mineralogical variations along the zonation sequence, a different D value can be calculated for each pegmatite zone. The influence of accessory minerals (zircon, monazite and apatite) on alkali metal fractionation is negligible due to their very low alkali metal partition coefficients (e.g. Klemme, 2003) and their overall low mass proportions in the Gatumba pegmatites.

These phases are consequently not incorporated in the alkali metal fractionation model.

5.2.2. Quantitative evidence of fractional crystallisation

Crystal/melt partitioning coefficients for alkali metals relevant for granites and pegmatites are relatively well constrained and have been compiled by Long (1978), Jolliff et al. (1992) and London (2005b), among others. An averaged G4-granite composition for K (3.1 wt%), Rb (222 ppm) and Cs (11 ppm) is used as initial concentration for the fractionation modelling in order to test the G4-parental, syngenetic origin for the Gatumba regionally zoned pegmatite field. These concentrations are representative for average alkali metal abundances in peraluminous, S-type granites (e.g. Chappell and White, 1992). The

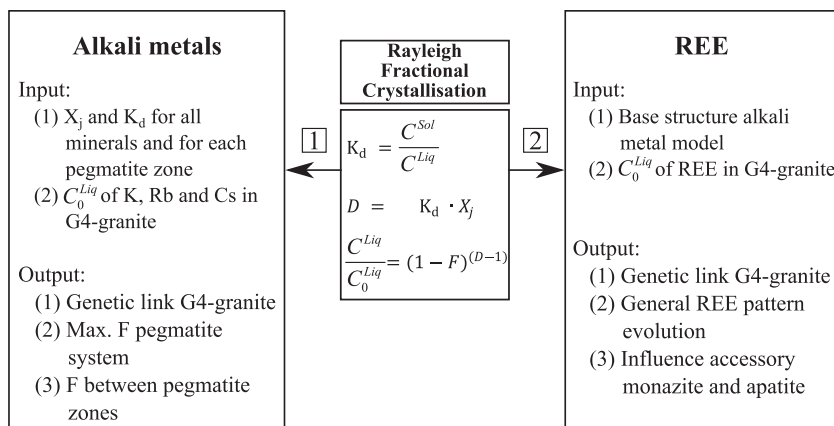


Fig. 9. Conceptual outline of the Rayleigh fraction model. The model is based on the Nernst crystal/melt partition coefficient (K_d) and bulk distribution coefficient (D). Both coefficients are used as input in the equation of Rayleigh for fractional crystallisation together with the concentration of the trace element in the parental melt before any crystallisation has occurred (C_0^{Liq}) and the mineral mass fractions for each pegmatite zonation (X_j). The degree of fractionation (F), expressed as the fraction of crystallised phases, is modelled as a variable. The intended trace element concentration in the mineral of interest (C^{Sol}) is recalculated from the concentration in the fractionated melt (C^{Liq}) by use of the partition coefficient. See also Section 5.1. for parameter definitions.

forward model methodology, as described in Section 5.2.1 and Fig. 9, is applied to verify and model the observed continuous fractionation trajectories of K/Rb versus Rb and K/Cs versus Cs in K-feldspars and muscovites (Fig. 10). At each step of fractional crystallisation the concentrations of K, Rb and Cs are calculated for all minerals crystallising in the system. By comparison of the modelled mineral concentrations with the analytical concentration data, characteristic values for the degrees of fractionation between the individual pegmatite zones as well as for the entire Gatumba pegmatite field can be obtained (Fig. 10). The observed mineralogical zonation in the Gatumba area can be explained by a single Rayleigh fractional crystallisation trajectory starting from a G4-granite initial composition. Biotite pegmatites crystallise between $F = 0$ and $F = 0.69 \pm 0.04$. Two-mica pegmatites are fractionation products ranging from $F = 0.69 \pm 0.04$ to $F = 0.92 \pm 0.02$. Muscovite pegmatites are marked by fractionation degrees between 0.92 ± 0.02 and 0.980 ± 0.004 . In order to model the extreme enrichment of Rb and Cs observed in mineralised pegmatites, the system has to differentiate to $F > 0.98$. The reported standard deviation is based on the comparison of the calculated F values for Rb with the calculated F values for Cs both in K-feldspar and muscovite. The incremental degree of enrichment of Rb and Cs in the melt and crystallising minerals is fairly low at low to intermediate degrees of fractionation, causing a relative higher degree of uncertainty on the modelled F values (Fig. 11). The exact curvature of the alkali metal fractionation trajectories, as can be observed in Fig. 10, is caused by the variation in the bulk mineralogy of the different pegmatite zones (Table 5). Especially the mica evolution from biotite, over biotite together with muscovite to solely muscovite is responsible for the specific shape of the continuous trajectories.

In addition to concentration calculations in solid phases, the forward model is applied to infer the alkali

metal evolution of the residual melt. Our model is conceptually based on concentration variations in minerals. This approach relies on the fact that primary magmatic minerals are sensitive to record the liquidus evolution of the pegmatite system compared to bulk geochemical data. Calculated residual melt concentrations of Rb and Cs for the Gatumba system (which has a starting concentration of 3.1 wt% K, 222 ppm Rb and 11 ppm Cs; cf. Table 5) are shown in Fig. 11. The bulk distribution coefficients for the different pegmatite zones vary from 0.52, 0.50 to 0.48 for Rb and 0.11, 0.10 to 0.07 for Cs. Modelled K residual melt concentrations are rather constant (C_0^{Liq} of 3.10 wt% to C^{Liq} of 3.06 wt% at 98% fractionation) due to near unity bulk distribution coefficients (~ 1.0035).

As stated in Section 5.1., Eqs. (11) and (12) allow calculating the K/Rb versus Cs trend for K-feldspar consistent with fractional crystallisation and as a function of the applied model parameters specific for the Gatumba pegmatite system. Fig. 8 shows these linear relationships for the logarithmic transformed K/Rb ratio versus Cs concentrations in K-feldspar, both for analytical data and for calculated data from the alkali fractionation model parameters. Slope (A) and y-intercept (B) are calculated as a function of K_d , D and C_0^{Sol} of K, Rb and Cs in K-feldspar and compared with the line parameters of the linear regression through the analytical data points (Fig. 8). Minimal and maximal values for A and B have been calculated for the reason that D for Rb and Cs decreases in some extent along the pegmatite zonation due to the variations in mineralogy (i.e. 0.48 versus 0.52 for Rb and 0.07 versus 0.11 for Cs). However these minor variations in D are insignificant for the calculated line parameters. The strong correlation (overlap) between the analytical and calculated K/Rb versus Cs trends confirms the petrogenetic significance of the model parameters K_d (compiled from literature data), C_0^{Sol} (concentration in parental G4-granite) and D (calculated with the fraction-

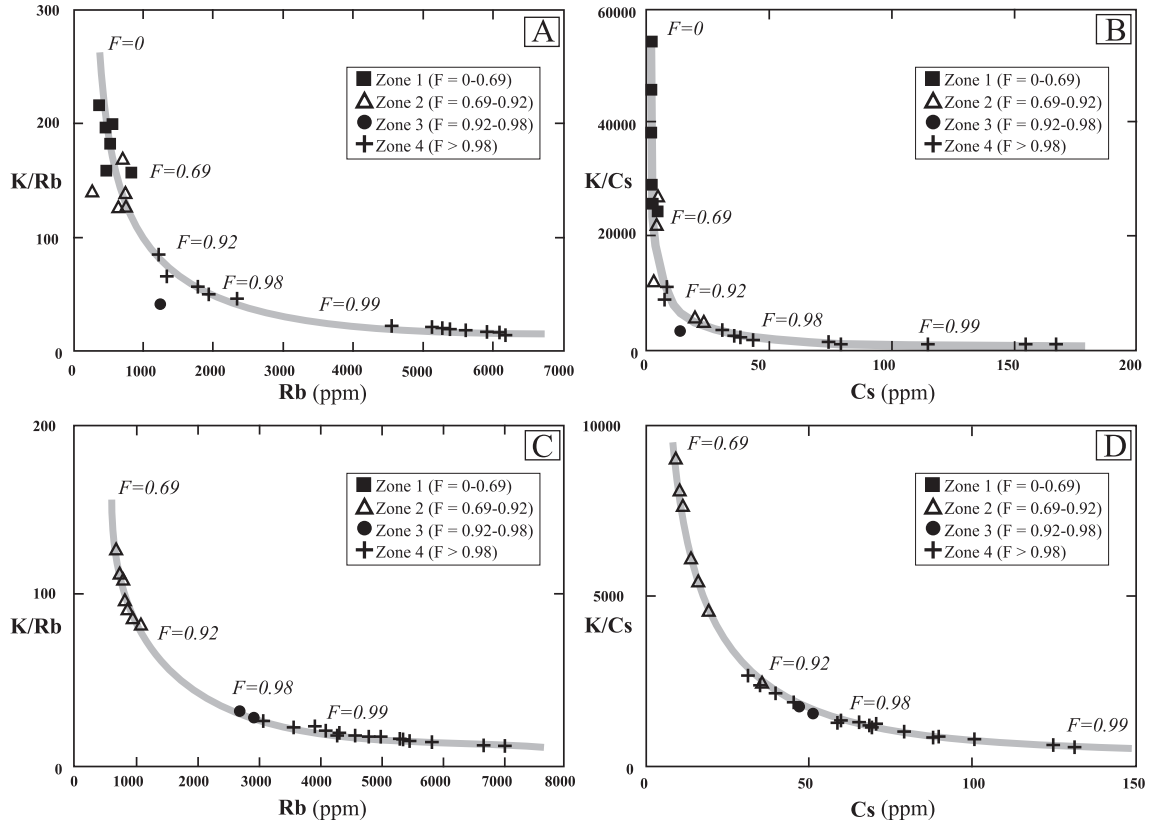


Fig. 10. Modelled Rayleigh fractionation trajectories for alkali metal trends in K-feldspars (A and B) and muscovites (C and D) along the zonation sequence (zone 1 = biotite pegmatites, zone 2 = two-mica pegmatites, zone 3 = muscovite pegmatites and zone 4 = mineralised pegmatites). The resulting degrees of fractionation are reported for the different pegmatite zones (ratios expressed in ppm/ppm).

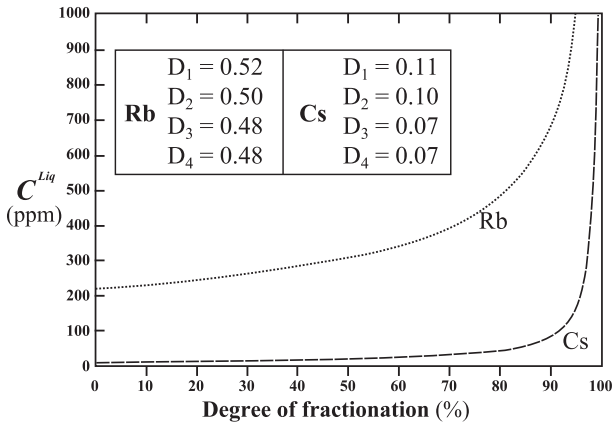


Fig. 11. Modelled Rayleigh fractionation curves of Rb and Cs in the residual melt (C^{Liq}) as a function of the degree of fractionation. The curves incorporate the mineralogical evolution of the pegmatite zonation from biotite (0–69%), two-mica (69–92%), muscovite (92–98%) to mineralised pegmatite (> 98%) zones by means of the evolution in the distribution coefficient D_1 , D_2 , D_3 and D_4 , respectively.

ation model) specific for the Gatumba pegmatite field and assure the robustness of the fractionation model itself.

5.3. Application of fractional crystallisation to REE

5.3.1. REE pattern systematics

Information on the REE concentration in the bulk and/or rock-forming minerals of common and rare-element pegmatites is in general very limited because of the difficulty to analyse representative sample aliquots and the overall low REE concentration in these types of rocks (Černý, 1997). Indeed all rock-forming minerals analysed from the Gatumba pegmatites are marked by low REE contents and low REE partition coefficients (cf. Nash and Crecraft, 1985; Bea et al., 1994a; Adam and Green, 2006). Feldspars are in general characterised by REE partition coefficients below unity and a decrease from LREE to HREE defining a fractionated pattern, except for Eu^{2+} which is readily accommodated at the alkali-site (Nash and Crecraft, 1985; Larsen, 2002). Biotite shows a slight preference for HREE, however, with lower than unity partition coefficients for peraluminous granitic compositions (e.g. Bea et al., 1994a). Nash and Crecraft (1985) reported biotite partition data for a rhyolitic composition that show a slight preference of biotite for LREE; some of the highest K_d values are even greater than unity. White mica tends to be in general a very poor host for REE (Adam and Green, 2006) and usually have lower REE contents than coexisting biotite (Laul and Lepel, 1987). Tourmaline partition

coefficient data are scarce but seem to be low (Jolliff et al., 1987; Laul and Lepel, 1987; van Hinsberg, 2011).

In general, minerals (i.e. biotite, muscovite, K-feldspar, plagioclase and schorl) from the Gatumba biotite pegmatites commonly display moderately to highly HREE-depleted patterns. This distribution of REE is inherited from the initial parental pegmatite-forming melt (cf. Miller and Mittlefehldt, 1984; Jefferies, 1985; Shearer et al., 1992; Bea et al., 1994b; Neiva and Ramos, 2011), i.e. in Rwanda the G4-granite generation (average composition in Table 5; see also Table 1), and reflected in the mineral REE partition coefficients (Table 5). The G4-granites in Rwanda display REE patterns characteristic for granites parental to rare-element pegmatites, i.e. moderately to slightly HREE-depleted patterns and low REE abundances ($La \sim 15-1$, $Yb \sim 2-0.2$; Černý, 1997). Conceptually, bulk REE distribution coefficients appear significantly lower than unity resulting in REE enrichment in the residual melt during differentiation, especially since quartz, micas and feldspars make up more than 75% of the pegmatitic rocks (cf. Schnetzler and Philpotts, 1970; Nash and Crecraft, 1985; Adam and Green, 2006). Advancing differentiation causes parallelism in the REE patterns. Progressive enrichment and pattern parallelism is observed in biotite from biotite pegmatites. The parallelism of the pattern requires a well-balanced assemblage of major and accessory minerals with the same distribution coefficients for all elements throughout differentiation (Cameron and Cameron, 1986; Evans and Hanson, 1993).

From the two-mica pegmatites onwards, the mineral patterns flatten or become somewhat MREE-enriched, in case of biotite due to the preferential depletion of the LREE-segments. Monazite is petrographically observed in the two-mica pegmatite zone and in the subsequent muscovite zone (Hulsbosch et al., 2013). Accessory monazite precipitation is interpreted to be responsible for the progressive LREE-depletion of the differentiating melts due to the extremely high REE crystal/melt partition coefficients and its LREE-preference (Evans and Hanson, 1993; Yurimoto et al., 1990; Bea et al., 1994a; Duke et al., 1992; Larsen, 2002). LREE-depletion is evident starting from the two-mica pegmatites, but progressive enrichment and pattern parallelism is only observed for the HREE-segments as conceptually illustrated in Fig. 12. Minerals from muscovite pegmatites show an analogous REE-pattern evolution as described for the two-mica pegmatites with monazite stability causing the observed LREE-depletion.

Primary mineral assemblages in the mineralised pegmatites consisting of feldspar, muscovite and elbaite are all characterised by HREE-depleted, fractionated chondritic patterns. The mineral patterns are substantially more complex for muscovite. The most abundant REE-compatible phases in the mineralised pegmatites of Gatumba are apatite and minor zircon (cf. Bertossa, 1965, 1967; Dewaele et al., 2011; Hulsbosch et al., 2013). The mineralised pegmatite zone is characterised by a multifaceted accessory mineral assemblage (e.g. spodumene, beryl and columbite-group minerals) occurring together with the rock-forming minerals quartz, muscovite, feldspar and elbaite (e.g. Daltry and von Knorring, 1998).

5.3.2. Extension of the fractionation model to REE

To be acceptable, the fractional crystallisation model elaborated in Section 5.2. for the alkali elements must also be able to explain the observed REE variation in the minerals. However, here arises a difficulty. While the presence of accessory minerals such as zircon, monazite, apatite, etc. could be neglected for the treatment of the alkali elements, this is no longer allowed for the REE. The prominent decline in LREE during crystallisation of the minerals of the two-mica and muscovite pegmatites and the decline in HREE in the minerals from the mineralised pegmatite zone with differentiation cannot be attributed to fractional crystallisation of solely quartz, feldspar, micas and tourmaline. Moreover both distinct variations in REE pattern are petrographically correlated with the stabilisation of REE-enriched mineral phases. Subsequently, the Rayleigh fractionation model is extended to the REE by incorporation of accessory minerals and applied to assess whether mineral fractionation can cause the gradual REE evolution. The REE fractionation model uses the modelled degrees of fractionation derived from the alkali metal calculations. Namely, alkali metal modelling has constrained the specific degrees of fractionation corresponding to the different pegmatite zone and enables to correlate the stabilisation of accessory minerals with a certain interval of degrees of fractionation: monazite stability in the two-mica and muscovite pegmatites ($0.69 \leq F \leq 0.98$) and apatite stability in the mineralised pegmatites ($F \geq 0.98$). Zircon is observed to be stable in the G4-parental granites (Tack et al., 2010) as well as in the pegmatite system (Varlamoff, 1954, 1963) and consequently modelled throughout the whole fractionation trajectory.

The REE model requires as input the C_0^{Liq} of the REE in the parental G4-granite generation and REE partition coefficients (Table 5). Missing values in the published REE

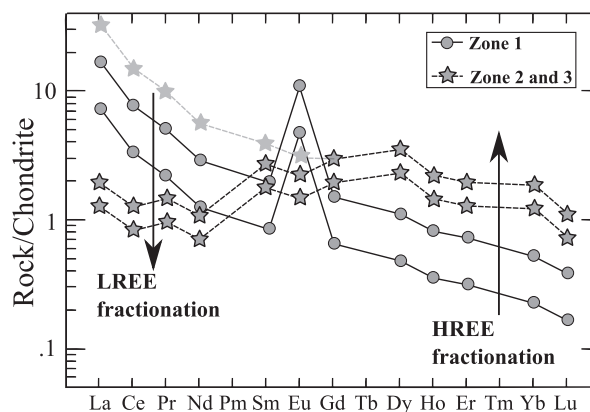


Fig. 12. Schematic evaluation of the influence of monazite stability on the evolution of the mineral REE patterns. Advancing melt differentiation, initially without monazite stability, causes the incompatible REE to be enriched in the evolving melt and crystallising rock-forming minerals (full patterns). The parallelism of the patterns requires a well-balanced assemblage of major and accessory minerals with the same distribution coefficients for all elements. Monazite stability in zones 2 and 3 (i.e. two-mica and muscovite pegmatites) causes a preferential depletion in LREE (dotted patterns).

coefficients are interpolated (cf. Irber, 1999) or assumed (cf. Jolliff et al., 1992). The behaviour of Eu is ignored in the further modelling because the preference of Eu^{2+} in feldspars and the $\text{Eu}^{2+}/\text{Eu}^{3+}$ ratio is dependent on oxygen fugacity (Drake, 1975). Moreover simple mineral fractionation results to be insufficient to budget the Eu content of the residual melt in the Gatumba system (cf. Graupner et al., 2010).

The main complexity in modelling the REE pattern evolution is the great variability in reported REE partition coefficients for the minerals of interest and applicable for evolved felsic melts, such as granites and pegmatites. REE partition coefficients for feldspars, micas and tourmaline are sensitive to changes in mineral composition and melt characteristics such as temperature, pressure, oxidation state, volatile content etc. (Mahood and Hildreth, 1983; Nash and Crecraft, 1985; Larsen, 2002; London, 2005b; Klemme et al., 2011; van Hinsberg, 2011) causing the reported REE partition coefficients to vary over an order of magnitude.

Quantitative crystal/melt trace element partitioning data are scarce in the case of tourmaline and white mica. Van Hinsberg (2011) reported preliminary experimental data on REE partitioning between tourmaline and silicate melt. He stated that tourmaline does not fractionate specific trace elements from melts. In addition, Klemme et al. (2011) reported REE partitioning coefficients between white mica and tourmaline to be close to one (except for La and Ce). These authors also concluded that tourmaline monitors the changes in the REE composition of the fluid/melt rather than causing them. Laul and Lepel (1987) suggested that tourmaline partition coefficients are low based on the low REE concentrations in tourmaline. Consequently, tourmaline and white mica REE partition coefficients are assumed according to the data of van Hinsberg (2011) and Adam and Green (2006). In addition, partition coefficients for rocks types representative for a felsic granitic and pegmatitic composition have been applied (e.g. rhyolites from Schmetzler and Philpotts, 1970 and Nash and Crecraft, 1985; peraluminous granites from Bea et al., 1994a).

The results of the simulation of the REE pattern evolution for the different rock-forming minerals by Rayleigh fractionation are shown in Fig. 13A–E. Similar to the alkali metal model, an averaged G4-granite composition has been used as initial concentration in the calculations (Table 5). Modelled patterns for the minerals of the early crystallising pegmatites, resembling biotite pegmatites ($F = 0\text{--}0.69$), show a sloping curve with a depleted HREE-segment. They show similarities in shape with the initial, parental bulk G4-granite pattern due to the non-fractionated behaviour of these minerals for the LREE and HREE. The total REE concentration in the minerals, correlating with low degrees of fractionation ($F < 0.69$), is in general lower than in the initial G4-composition due to their REE incompatibility. Muscovite and related monazite stability is modelled starting from $F = 0.69$ up to 0.98, representing the two-mica and muscovite pegmatites. With the introduction of monazite in the system, a systematic lowering of the LREE-segments is observed whilst the HREE-segments increase and show the typical parallelism (e.g. biotite in Fig. 13C) pointing to a

still well-balanced mineral assemblage for the parallelism in HREE. Consequently a more flat, non-fractionated pattern is obtained for minerals from the two-mica and muscovite pegmatites zones ($0.69 \leq F \leq 0.98$). Mineralised pegmatites are modelled to be equivalent to $F > 0.98$ and the REE-evolution is influenced by the stability of apatite. The introduction of apatite in the model causes the depletion in (MREE and) HREE, whilst the LREE-segments become relatively more enriched. As such, the overall flat to LREE-depleted mineral patterns, typically for monazite stability in the two-mica and muscovite pegmatites, changes back to more HREE-depleted and fractionated mineral pattern in the mineralised pegmatites due to preferential incorporation of HREE (and MREE) by apatite. The fractionation model demonstrates that the observed REE pattern evolution can theoretically be produced by fractional crystallisation of an initial melt with G4-composition consistent with the alkali metal variations in the Gatumba pegmatite system.

6. IMPLICATIONS FOR RARE-ELEMENT PEGMATITE FORMATION

6.1. Model evaluation

The fractionation model is based on the evolution of a relative simple mineralogy in the biotite, two-mica and muscovite pegmatite zones evolving to a more complex mineralogy in the mineralised pegmatites. The three former zones are characterised by feldspar–quartz–mica with mineral modes higher than 75%. The mineralised pegmatites, consist also of apatite, multi-coloured and white beryl, spodumene, elbaite, columbite–tantalite and other accessory phases (see Section 2.2.). As such, our Rayleigh fractionation model assumes a general simplification of the bulk mineralogy of the mineralised pegmatites. This simplification is rather insignificant for the alkali metal modelling, because biotite, muscovite and feldspars, representing the main alkali metal carriers in a pegmatitic environment (London, 2005b), are fully incorporated in the model. In the case of the REE model only monazite and apatite are incorporated as REE-fractionating minerals, because they are the main accessories and relatively well characterised in terms of their crystal/melt partition coefficients (Miller and Mittlefehldt, 1982; Yurimoto et al., 1990; Zhao and Cooper, 1992; Bea et al., 1994a). Jolliff et al. (1987) reported, moreover, that columbite-group minerals and beryl may also depress the HREE-segments (cf. Graupner et al., 2010 for the Gatumba area pegmatites). In essence, the co-occurrence of these HREE-depressing minerals is modelled solely by apatite stabilisation because quantitative partition data for beryl and columbite-group minerals is lacking. Mineral fractionation by the phosphates monazite and apatite seem to be an effective mechanism in order to generate the first-order REE pattern evolution observed in the rock-forming minerals of the Gatumba pegmatite.

The inability of our Rayleigh fractionation to model the Eu-anomaly along the zonation sequence (see Section 5.3.) indicates that simple mineral fractionation by feldspars cannot be held exclusively responsible for the origin of

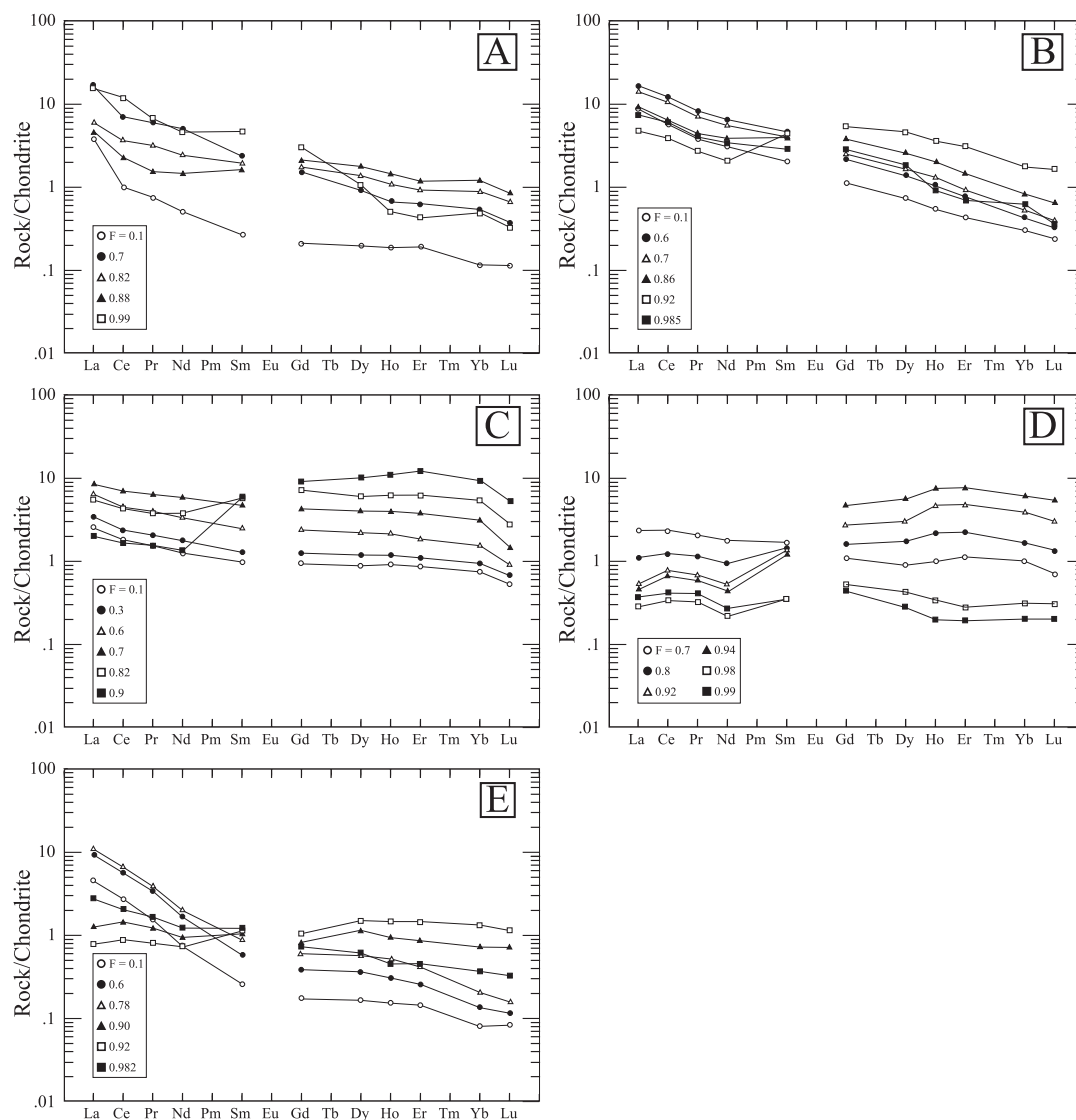


Fig. 13. REE pattern changes modelled for primary minerals by Rayleigh fractional crystallisation and with the stabilisation of monazite in the two-mica ($F = 0.69$ – 0.92) and muscovite pegmatites ($F = 0.92$ – 0.98); and apatite in de mineralised pegmatites ($F > 0.98$). (A) K-feldspar (B) plagioclase, (C) biotite, (D) muscovite and (E) tourmaline.

the Eu-anomaly (cf. Irber, 1999). Also a direct evolution to a more oxidising melt (higher oxygen fugacity) with protracting fractionation can not be proposed as the driving process. More oxidising conditions would result in a declining $\text{Eu}^{2+}/\text{Eu}^{3+}$ ratio starting from the biotite up to the mineralised pegmatites. This would cause the formation of less Eu-bearing K-feldspar or plagioclase with ongoing differentiation which in turn results in a less-pronounced negative Eu-anomaly for Eu^{2+} -incompatible phases such as biotite and muscovite (Drake, 1975; Irber, 1999). Trivalent Eu shows similar incompatibility as the other REE^{3+} and should, therefore, be more likely partition in the melt. This combined effect is not observed for the Gatumba

sequence: feldspars and micas shows both a declining Eu-anomaly. A complex combination of processes such as feldspar fractionation, redox shifts possibly together with melt structure variations (Eu^{2+} -aluminosilicate complexes; Möller and Muecke, 1984) are thought to be responsible for the observed Eu-anomaly variations (cf. Graupner et al., 2010).

6.2. Fractional crystallisation: a syngenetic granite–pegmatite system

The alkali metal fractionation modelling indicates that the Gatumba pegmatite field can be explained geochemically by one continuously differentiating magmatic system

driven by extreme Rayleigh fractional crystallisation from a parental composition which corresponds to a regional G4-granite composition (Figs. 8, 10 and 11). Deciphering fractional crystallisation as the main mechanism for extreme chemical differentiation (cf. Černý et al., 2005), is the key for understanding the genesis of the G4-granite/pegmatite system. Varlamoff (1972; and older references therein), Pohl (1994) and Dewaele et al. (2011) identified the G4-granites as the parental granites for rare-element pegmatites located in the KAB based on temporal and spatial relationships. As such, the alkali metal modelling shows that also a geochemical, syngenetic relationship can be inferred for the G4-granites and their associated pegmatites. The correlation of the regional zonation with a geochemical differentiation trajectory is also recorded by the variations in mineral composition along the Gatumba pegmatite zonation sequence (Hulsbosch et al., 2013). Biotites are characterised by an increase of the $Fe_{tot}/(Fe_{tot} + Mg)$ ratio and a decrease in the Mg, Mn and Ti content along the zonation (Hulsbosch et al., 2013). The variation in tourmaline solid-solution follows the regional fractionation trend in the Gatumba pegmatite field. Black schorl records an evolution from Mg-rich schorl in biotite pegmatites to Mg-poor schorl in muscovite pegmatites with an intermediate Mg-content for the two-mica pegmatites. Elbaite with an increased Mn content stabilised in the mineralised pegmatites. With increasing chemical fractionation of the pegmatitic melt, the composition of tourmaline evolves from dravite- to schorl-rich. The stability of schorl depleted the system mostly in mafic components such as Fe, Mg and Ti. Prolonged fractionation also raised the Li content to the level required to stabilise the formation of elbaite (and spodumene) in the most evolved, distal mineralised pegmatites (Hulsbosch et al., 2013).

The quantitative evaluation of the trace element evolution along regionally zoned pegmatite groups combined with fractionation modelling provides strong evidence in favour of the extraction of an incompatible element enriched melt from a common granite body. The mechanism of Rayleigh-type fractional crystallisation confirms that granitic pegmatites are genetically connected to the main granite body. However, several end-member fractionation mechanisms are proposed for the formation of regional zonation in a pegmatite field (e.g. Shearer et al., 1992; Mulja et al., 1995; London, 2008; Simmons and Webber, 2008; Thomas and Davidson, 2013). Hulsbosch et al. (2013) suggested that a scenario involving a sequential and pulsed tapping from an evolving G4-pluton can be excluded for the Gatumba area since this sequential tapping would imply cross-cutting relations between individual pegmatites of different zones and the lack of a concentric zoning in the field (cf. Dewaele et al., 2011). The simultaneous chemical fractionation scenario in an open system over the entire occurrence of the G4-pegmatite complex, is also unlikely (Hulsbosch et al., 2013; cf. London, 2008). The different pegmatite zones of the Gatumba area demonstrate a single path of geochemical evolution based on various mineralogical (e.g. evolution from schorl to elbaite along zonation) and geochemical (e.g. $Fe_{tot}/(Fe_{tot} + Mg)$ of biotite and tourmaline, K/Rb and

K/Cs in feldspars and micas, fractionation modelling) proxies. In addition, the field relationships indicate that the pegmatite dikes are not a continuous feature. The pegmatites occur as individual dikes with various dimensions and a clear and unique mineralogical composition (Varlamoff, 1954). Consequently, an open system fractionation seems less plausible because this scenario would require that the distal pegmatite-forming melts remain interconnected with the main body of the G4-granite throughout the entire time period of pegmatite formation. A more practical situation for the Gatumba area involves a third scenario suggested by London (2005a,b, 2008), i.e. the existence of a chemical zonation within the G4-source pluton prior to the pegmatite emplacement (cf. Michael, 1983; Shearer et al., 1992; Bea et al., 1994b; Mulja et al., 1995; Simmons and Webber, 2008). Nonetheless, still several processes are proposed for the geochemical specialisation of the G4-granites, such as prolonged magmatic differentiation and fractional crystallisation at depth (Lehmann, 1987; Lehmann and Lavreau, 1988), with combined hydrothermal fluid interaction (Lehmann and Lavreau, 1987), and crustal thickening and re-melting of restites of earlier granites (Günther et al., 1989; Pohl, 1994). In general, processes such as early side-wall crystallisation of the initial granitic melt and continued fractional crystallisation can produce a geochemical specialised pluton with successive differentiated melt compositions (Mulja et al., 1995). Late-stage expulsion of a volatile-rich melt from the magma chamber owing to fluid overpressure, and further expulsion of the highly-evolved pegmatite-forming melts by pluton contraction due to advancing crystallisation and cooling, have the potential to result in the observed pegmatite zonation (Baker and McBirney, 1985; McBirney et al., 1985).

Recently, Thomas and Davidson (2012, 2013) and Thomas et al. (2012) delivered new detailed insights regarding the separation of pegmatite-forming melts from the parental, granite melts. They concluded that melt inclusions in granite minerals, for which their composition deviates from the bulk rock chemistry, represent the residual, intergranular melt enriched in incompatible elements. This residual melt has typical high volatile and melt structure modifier concentrations (e.g. F, B, P, alkali metals, carbonates, sulphates, borates, phosphates and H_2O), causing the melt viscosity to be several orders of magnitude lower than the crystal mush matrix (Thomas et al., 2012). This advanced compositional and physical differentiations between a low-viscous, residual melt and its parental melt are realistic conditions to extract the pegmatite-forming melt from the granite matrix (McKenzie, 1985; Thomas and Davidson, 2013). Essentially, our contribution provides evidence that Rayleigh-type fractional crystallisation is the main differentiation process responsible for the advanced compositional differentiation and the formation of an incompatible element enriched, residual melt. Additional experimental and physicochemical investigations (e.g. melt and fluid inclusions) of this dynamic melt evolution (i.e. low viscous melts, melt–melt–fluid immiscibility, formations of extremely evolved melt fractions etc.) along regionally zoned pegmatite fields is needed to fully understand the general question

of when and how pegmatites and more evolved melts are derived from the source granite. This research is in progress in the Gatumba area.

7. SUMMARY AND CONCLUSION

The recognition of Rayleigh fractional crystallisation as a principal differentiation mechanism in pegmatite petrogenesis allows evaluation and quantification of the essential petrogenetic parameters for granite–pegmatite differentiation series (i.e. initial element concentrations in the parental granitic melt, mineral–melt partition coefficients, bulk distribution coefficients and degrees of fractionation) on the basis of trace element data. The regional pegmatite zonation in the Gatumba area comprises four distinct zones around a G4-granite pluton. Common pegmatites rich in schorl occur proximal in the zonation. Outwardly they grade into biotite (zone #1), two-mica (zone #2) and muscovite (zone #3) pegmatites. Rare-metal, Nb–Ta–Sn mineralised pegmatites (zone #4) are formed most distal in the zonation sequence. Supporting evidence from mineral geochemistry indicated that, with the evolution of the pegmatite system, biotite and tourmaline show a general decrease in mafic components along the zonation (e.g. Fe, Mg and Ti) which corresponds with mineral fractionation. This initial assessment of major and trace element data warrants the more elaborated modelling of Rayleigh fractional crystallisation in the formation of regionally zoned pegmatite groups.

Alkali element and REE concentrations of feldspar, mica and tourmaline are sensitive indicators of the magmatic evolution of pegmatites. In particular, their systematic variations constrain the degree of differentiation of the residual, pegmatite-forming melt and the relationships among the different pegmatite zones within a regionally zoned pegmatite group. In order to model these variations in terms of a differentiating G4-granite/pegmatite system, the initial pegmatite melt trace element concentrations are estimated from a regionally averaged G4-granite composition. This granite generation is thought to be parental to the pegmatite system due to spatial and temporal (granite and pegmatite emplacement ages of 986 ± 10 Ma and 969 ± 8 Ma, respectively; Tack et al., 2010; Brinckmann and Lehmann, 1983) relationships. Its inferred model composition is: 3.1 wt% K, 222 ppm Rb, 11 ppm Cs; REE contents are rather low ($\sum \text{REE} \sim 83$), and HREE-depleted ($\text{La}_N/\text{Yb}_N \sim 10$) and characteristic for granites parental to rare-element pegmatites. Observed and Rayleigh-modelled rare alkali metal concentrations in K-feldspar and mica demonstrate a ‘power-law’-type behaviour, i.e. Rb and Cs concentrations increase from the proximal pegmatite zones through the last-evolved, distal zones. This inter-pegmatite variability for the alkali metals can be quantified by a continuous fractional crystallisation trajectory, resembling a regional and spatial differentiation trend starting from the parental granite up to most fractionated, rare-element pegmatites. More specifically, Rayleigh fractionation modelling showed that biotite pegmatites crystallise during fractionation from 0% to 69%, two-mica pegmatites from 0.69% to 92% and muscovite pegmatites are high

fractionation products (at least 92%). The extreme Rb- and Cs-enrichment in the rare-element pegmatites originates from fractionation of more than 98% of the initial G4-granite composition. As recorded by feldspars, micas and tourmaline samples, the REE (except for Eu^{2+}) firstly behave incompatibly in this pegmatite system, as expressed by the parallel shift of the REE patterns of similar minerals for each pegmatite zone. Changes in the shape of the REE patterns originate from early crystallisation of the LREE “sink” monazite and from late crystallisation of HREE-preferring phases such as apatite, and possibly also cogenetic columbite-group minerals and beryl.

The quantitative integration of alkali metal and REE data provides a detailed reconstruction of the magmatic evolution of a regionally zoned pegmatite field evolving from a biotite over a two-mica and muscovite pegmatite zone to a (Nb–Ta–Sn) mineralised pegmatite zone. Extensive Rayleigh-type fractionation, starting from a G4-granite composition, is responsible for the regional-scale, mineralogical and geochemical zonation of pegmatite groups. Rayleigh fractional crystallisation provides a mechanism by which small proportions of highly differentiated melts can originate and evolve starting from a granitic parental composition. These residual melts are significantly enriched in incompatible elements, acting as melt structure modifiers (e.g. alkali metals, B, P, F, H_2O etc.), and resulting in mobile, low viscous melts. These enhanced physicochemical conditions are required to extract the residual, pegmatite-forming melts from the nearly solidified, granitic mush.

ACKNOWLEDGEMENTS

Research of Niels Hulsbosch is funded by a Ph.D. grant of the Agency for Innovation by Science and Technology (IWT). We would like to express our gratitude to Dr. Elvira Vassilieva for her help with the ICP-OES analyses and Herman Nijs for preparing the thin sections. We would also like to thank Jacques Navez and Laurence Monin of the RMCA for the assistance with the ICP-QMS analyses. This manuscript benefited from insightful and constructive reviews provided by Prof. Dr. Bernd Lehmann and Dr. Rainer Thomas. We are grateful to Executive Editor Dr. Marc Norman for his comments and editorial handling.

REFERENCES

- Adam J. and Green T. (2006) Trace element partitioning between mica- and amphibole-bearing garnet lherzolite and hydrous basaltic melt: 1. Experimental results and the investigation of controls on partitioning behaviour. *Contrib. Mineral. Petrol.* **152**, 1–17.
- Alfonso A. P. and Melgarejo J. C. (2008) Fluid evolution in the zoned rare-element pegmatite field at Cap de Creus, Catalonia, Spain. *Can. Mineral.* **46**, 597–617.
- Alfonso A. P., Melgarejo J. C., Yusta I. and Velasco F. (2003) Geochemistry of feldspars and muscovite in granitic pegmatite from Cap de Creus field, Catalonia, Spain. *Can. Mineral.* **41**, 103–116.
- Baudet D., Hanon M., Lemonne E., Theunissen K., Buyagu S., Dehandschutter J., Ngizimana W., Nsengiyumva P., Rusanganwa J. B. and Tahon A. (1988) Lithostratigraphie du domaine sédimentaire de la chaîne Kibarienne au Rwanda. *Ann. Soc. Geol. Belg.* **112**, 225–246.

- Baker B. H. and McBirney A. R. (1985) Liquid fractionation. Part III: Geochemistry of zoned magmas and the compositional effects of liquid fractionation. *J. Volcanol. Geotherm. Res.* **24**, 55–81.
- Bea F., Pereira M. D. and Stroh A. (1994a) Mineral/leucosome trace-element partitioning in a peraluminous migmatite (a laser ablation-ICP-MS study). *Chem. Geol.* **117**, 291–312.
- Bea F., Pereira M. D., Corretgé L. G. and Fershtater G. B. (1994b) Differentiation of strongly peraluminous, perphosphorus granites. The Pedrobernardo pluton, central Spain. *Geochim. Cosmochim. Acta* **58**, 2609–2628.
- Bertossa A. (1965) Geologisch-Erzlagerstättenkundliche Notiz über Rwanda. *Bull. Serv. Geol. Rwanda* **3**, 5–18.
- Bertossa A. (1967) Inventaire des minéraux du Rwanda. *Bull. Serv. Geol. Rwanda* **4**, 25–45.
- Brinckmann J. and Lehmann, B. (1983) Exploration de la bastnaésite-moncite dans la région de Gakara, Burundi. Bujumbura – Hannover.
- Cahen L. (1964) État de la géochronologie du Rwanda. *Bull. Serv. Geol. Rwanda* **1**, 35–38.
- Cahen L. and Ledent D. (1979) Précisions sur l'âge, la pétrogénèse et la position stratigraphique des granites à étain de l'est de l'Afrique Centrale. *Bull. Soc. Belge. Geol.* **88**, 33–49.
- Cahen L., Snelling N. J., Delhal J., Vail J. R., Bonhomme M. and Ledent D. (1984) *The Geochronology and Evolution of Africa*. Clarendon Press, Oxford.
- Cameron K. L. and Cameron M. (1986) Whole-rock/groundmass differentiation trends of rare earth elements in high-silica rhyolites. *Geochim. Cosmochim. Acta* **50**, 759–769.
- Canosa F., Martin-Izard A. and Fuentès-Fuente M. (2012) Evolved granitic systems as a source of rare-element deposits: the Ponte Segade case (Galicia, NW Spain). *Lithos* **153**, 165–176.
- Černý P. (1991a) Rare element granitic pegmatites. Part I: Anatomy and internal evolution of pegmatite deposits. *Geosci. Can.* **18**, 29–47.
- Černý P. (1991b) Rare-element granitic pegmatites. Part II: Regional to global environments and petrogenesis. *Geosci. Can.* **18**, 49–62.
- Černý P. (1997) REE trends in rare-element granitic pegmatites: enrichment vs. depletion in granite-to-pegmatite sequences. *J. Czech. Geol. Soc.* **42**, 34.
- Černý P. and Ercit T. S. (2005) The classification of granitic pegmatites revisited. *Can. Mineral.* **43**, 2005–2026.
- Černý P., Trueman D. L., Ziehle D. V., Goad B. E. and Paul B. J. (1981) *The Cat Lake – Winnipeg River and the Wekusko Lake pegmatite fields, Manitoba*. Manitoba Dep. Energy Mines, Miner. Resour. Div., Econ. Rep. **ER80-1**.
- Černý P., Meintzer R. E. and Anderson A. J. (1985) Extreme fractionation in rare element granitic pegmatites: selected examples of data and mechanism. *Can. Mineral.* **23**, 381–421.
- Černý P., Blevin P. L., Cuney M. and London D. (2005) Granite-Related Ore Deposits. *Econ. Geol.* **100th Anniv.**, 337–370.
- Černý P., London D. and Novák M. (2012a) Granitic pegmatites as reflections of their sources. *Elements* **8**, 289–294.
- Černý P., Corkery M. T., Halden N. M., Ferreira K., Brisbin W. C., Chackowsky L. E., Meintzer R. E., Longstaffe F. J. and Trueman D. L. (2012b) Extreme fractionation and deformation of the leucogranite-pegmatite suite at Red Cross Lake, Manitoba, Canada. I. Geological setting. *Can. Mineral.* **50**, 1793–1806.
- Černý P., Teertstra D. K., Chapman R., Selway J. B., Hawthorne F. C., Ferreira K., Chackowsky L. E., Wang X.-J. and Meintzer R. E. (2012c) Extreme fractionation and deformation of the leucogranite-pegmatite suite at Red Cross Lake, Manitoba, Canada. IV. Mineralogy. *Can. Mineral.* **50**, 1839–1875.
- Chappell B. W. and White A. J. R. (1992) I- and S-type granites in the Lachlan Fold Belt. *Trans. Roy. Soc. Edin. Earth Sci.* **83**, 1–26.
- Daltry V. D. C. and von Knorring O. (1998) Type-mineralogy of Rwanda with particular reference of the Buranga pegmatite. *Geol. Belg.* **1**, 9–15.
- De Clercq F., Muechez Ph., Dewaele S. and Boyce A. (2008) The tungsten mineralisation at Nyakabingo and Gifurwe (Rwanda): preliminary results. *Geol. Belg.* **11**, 251–258.
- De Waele B., Johnson S. P. and Pisarevsky S. A. (2008) Palaeoproterozoic to Neoproterozoic growth and evolution of the eastern Congo Craton: its role in the Rodinia puzzle. *Precambrian Res.* **160**, 127–141.
- Dewaele S., Tack L., Fernandez M., Boyce A., Muechez Ph., Schneider J., Cooper G. and Wheeler K. (2008) Geology and mineralisation of the Gatumba area, Rwanda: present state of knowledge. *Etud. Rwandaises* **16**, 6–24.
- Dewaele S., De Clercq F., Muechez P., Schneider J., Burgess R., Boyce A. and Fernandez Alonso M. (2010) Geology of the cassiterite mineralisation in the Rutongo Area, Rwanda (Central Africa): current state of knowledge. *Geol. Belg.* **13**, 91–112.
- Dewaele S., Henjes-Kunst S., Melcher F., Sitnikova M., Burgess R., Gerdes A., Fernandez Alonso M., De Clercq F., Muechez Ph. and Lehmann B. (2011) Late Neoproterozoic overprinting of the cassiterite and columbite-tantalite bearing pegmatites of the Gatumba area, Rwanda (Central Africa). *J. Afr. Earth Sci.* **61**, 10–26.
- Drake M. J. (1975) The oxidation state of europium as an indicator of oxygen fugacity. *Geochim. Cosmochim. Acta* **39**, 55–64.
- Duchesne J. C., Liégeois J. P., Deblond A. and Tack L. (2004) Petrogenesis of the Kabanga-Musongati layered mafic-ultramafic intrusions in Burundi (Kibaran Belt): geochemical, Sr–Nd isotopic constraints and Cr–Ni behaviour. *J. Afr. Earth Sci.* **39**, 133–145.
- Duke E. F., Papike J. J. and Laul J. C. (1992) Geochemistry of a Boron-rich peraluminous granite pluton: the calamity peak layered granite-pegmatite complex, Black Hills, South Dakota. *Can. Mineral.* **30**, 811–833.
- Evans O. C. and Hanson G. N. (1993) Accessory-mineral fractionation of rare-earth element (REE) abundances in granitoid rocks. *Chem. Geol.* **110**, 69–93.
- Fernandez-Alonso M., Lavreau J. and Klerck J. (1986) Geochemistry and geochronology of the Kibaran granites in Burundi, Central Africa: implications for the Kibaran Orogeny. *Chem. Geol.* **57**, 217–234.
- Fernandez-Alonso M., Tack L., Tahon A., Laghmouch M. and Hardy B. (2007) *Geological Compilation of the Mesoproterozoic Northeastern Kibara (Karagwe-Ankole) Belt*. RMCA, Tervuren, 1/500,000.
- Fernandez-Alonso M., Cutten H., De Waele B., Tack L., Tahon A., Baudet D. and Barrit S. D. (2012) The Mesoproterozoic Karagwe-Ankole Belt (formerly the NE Kibara Belt): the result of prolonged extensional intracratonic basin development punctuated by two short-lived far-field compressional events. *Precambrian Res.* **216**, 63–86.
- Gérards J. (1965) Géologie de la région de Gatumba. *Bull. Serv. Geol. Rwanda* **2**, 31–42.
- Gérards J. and Ledent D. (1970) Grands traits de la géologie du Rwanda, différents types de roches granitiques et premières données sur les âges de ces roches. *Ann. Soc. Geol. Belg.* **93**, 477–489.
- Goad B. E. and Černý P. (1981) Peraluminous pegmatitic granites and their pegmatite aureoles in the Winnipeg River District, Southeastern Manitoba. *Can. Mineral.* **19**, 177–194.
- Graupner T., Melcher F., Gäbler H.-E., Sitnikova M., Brätz H. and Bahr A. (2010) Rare earth element geochemistry of

- columbite-group minerals: LA-ICP-MS data. *Mineral. Mag.* **74**, 691–713.
- Greenland L. P. (1970) An equation for trace element distribution during magmatic crystallization. *Am. Mineral.* **55**, 455–465.
- Günther M. A., Dulski P., Lavreau J., Lehmann B., Möller P. and Pohl W. (1989) The Kibaran tin granites: hydrothermal alteration versus plate tectonic setting. *IGCP 255 Newslett* **2**, 21–27.
- Hanson G. N. (1978) The application of trace elements to the petrogenesis of igneous rocks of granitic composition. *Earth Planet. Sci. Lett.* **38**, 26–43.
- Hertogen J. and Gijbels R. (1976) Calculation of trace element fractionation during partial melting. *Geochim. Cosmochim. Acta* **40**, 313–322.
- Hulsbosch N., Hertogen J., Dewaele S., André L. and Muchez Ph. (2013) Petrographic and mineralogical characterisation of fractionated pegmatites culminating in the Nb-Ta-Sn pegmatites of the Gatumba area (western Rwanda). *Geol. Belg.* **16**, 105–117.
- Icenhower J. and London D. (1995) An experimental study of element partitioning among biotite, muscovite, and coexisting peraluminous silicic melt at 200 MPa (H₂O). *Am. Mineral.* **80**, 1229–1251.
- Icenhower J. and London D. (1996) Experimental partitioning of Rb, Cs, Sr, and Ba between alkali feldspar and peraluminous melt. *Am. Mineral.* **81**, 719–734.
- Irber W. (1999) The lanthanide tetrad effect and its correlation with K/Rb, Eu/Eu*, Sr/Eu, Y/Ho, and Zr/Hf of evolving peraluminous granite suites. *Geochim. Cosmochim. Acta* **63**, 489–508.
- Jefferies N. L. (1985) The Distribution of the rare earth elements within the Carnmenellis Pluton, Cornwall. *Mineral. Mag.* **49**, 495–504.
- Jolliff B. L., Papike J. J. and Shearer C. K. (1986) Tourmaline as a recorder of pegmatite evolution: Bob Ingersoll pegmatite, Black Hills, South Dakota. *Am. Mineral.* **71**, 472–500.
- Jolliff B. L., Papike J. J. and Shearer C. K. (1987) Fractionation trends in mica and tourmaline as indicators of pegmatite internal evolution: Bob Ingersoll pegmatite, Black Hills, South Dakota. *Geochim. Cosmochim. Acta* **51**, 519–534.
- Jolliff B. L., Papike J. J. and Shearer C. K. (1992) Petrogenetic relationships between pegmatite and granite based on geochemistry of muscovite in pegmatite wall zones, Black Hills, South Dakota, USA. *Geochim. Cosmochim. Acta* **56**, 1915–1939.
- Keller P., Roda-Robles E., Pesquera A. and Fontan F. (1999) Chemistry, paragenesis and significance of tourmaline in pegmatites of the Southern Tin Belt, central Namibia. *Chem. Geol.* **158**, 203–225.
- Klemme S. (2003) Trace element partitioning between apatite and carbonatite melt. *Am. Mineral.* **88**, 639–646.
- Klemme S., Marschall H. R., Jacob D. E., Prowatke S. and Ludwig T. (2011) Trace-element partitioning and boron isotope fractionation between white mica and tourmaline. *Can. Mineral.* **49**, 165–176.
- Kontak D. J. (2006) Nature and origin of an LCT-suite pegmatite with late-stage sodium enrichment, Brazil Lake, Yarmouth County, Nova Scotia. I. Geological settings and petrology. *Can. Mineral.* **44**, 563–598.
- Kontak D. J. and Kyser T. K. (2009) Nature and origin of LCT-suite pegmatite with late-stage sodium enrichment, Brazil Lake, Yarmouth County, Nova Scotia. II. Implications of stable isotopes ($\delta^{18}\text{O}$, δD) for magma source, internal crystallisation and nature of sodium metasomatism. *Can. Mineral.* **47**, 745–764.
- Larsen R. B. (2002) The distribution of rare-earth elements in K-feldspar as an indicator of the petrogenetic processes in granitic pegmatites: examples from two pegmatite fields in Southern Norway. *Can. Mineral.* **40**, 137–151.
- Laul J. C. and Lepel E. A. (1987) Rare earth elements patterns in biotite, muscovite and tourmaline samples. *J. Radioanal. Nucl. Chem. Ar.* **112**, 461–471.
- Lavreau J. and Liégeois J.-P. (1982) Granites à étain et granito-gneiss Burundiens au Rwanda (région de Kibuye): âge et signification. *Ann. Soc. Geol. Belg.* **105**, 289–294.
- Lehmann B. (1987) Tin granites, geochemical heritage, magmatic differentiation. *Geol. Rundsch.* **76**, 177–185.
- Lehmann B. and Lavreau J. (1987) Tin granites of the northern Kibaran belt, Central Africa (Kivu/Zaire, Rwanda, Burundi). In *Current Research in African Earth Sciences* (eds. G. Matheis and H. Schandelmeyer). Balkema, Rotterdam, pp. 33–36.
- Lehmann B. and Lavreau J. (1988) Geochemistry of tin granites from Kivu (Zaire), Rwanda and Burundi. *IGCP 255 Newslett.* **1**, 43–46.
- Lehmann B., Nakai S., Höhndorf A., Brinckmann J., Dulski P., Hein U. F. and Masuda A. (1994) REE mineralization at Gakara, Burundi: evidence for anomalous upper mantle in the western Rift Valley. *Geochim. Cosmochim. Acta* **58**, 985–992.
- Lehmann B., Halder S., Ruzindana Munana J., de la Paix N. and Biryabarema M., (2013) The geochemical signature of rare-metal pegmatites in Central Africa: Magmatic rocks in the Gatumba tin-tantalum mining district, Rwanda. *J. Geochem. Explor.*, Accepted for publication.
- Lentz D. (1992) Petrogenesis and geochemical composition of biotites in rare-element granitic pegmatites in the southwestern Grenville Province, Canada. *Miner. Petrol.* **46**, 239–256.
- Linnen R. L., Van Lichtervelde M. and Černý P. (2012) Granitic pegmatites as sources of strategic metals. *Elements* **8**, 275–280.
- London D. (2005a) Granitic pegmatites: an assessment of current concepts and directions for the future. *Lithos* **80**, 281–303.
- London D. (2005b) Geochemistry of alkalis and alkaline earths in ore-forming granites, pegmatites, and rhyolites. In *Rare-Element Geochemistry of Ore Deposits* (eds. R. Linnen and I. Sampson). Geol. Assoc. Can. Short Course Notes 17. pp. 17–43.
- London D. (2008) *Pegmatites*. MAC, Quebec.
- London D. (2014) A petrological assessment of internal zonation in granitic pegmatites. *Lithos* **184–187**, 74–104.
- London D. and Morgan G. B. (2012) The pegmatite puzzle. *Elements* **8**, 263–268.
- Long P. E. (1978) Experimental determination of partition coefficients for Rb, Sr, and Ba between alkali feldspar and silicate liquid. *Geochim. Cosmochim. Acta* **42**, 833–846.
- Mahood G. A. and Hildreth E. W. (1983) Large partition coefficients for trace elements in high-silica rhyolites. *Geochim. Cosmochim. Acta* **47**, 11–30.
- McBirney A. R., Baker B. H. and Nilson R. H. (1985) Liquid fractionation. Part I: Basic principles and experimental simulations. *J. Volcanol. Geotherm. Res.* **24**, 1–24.
- McKenzie D. (1985) The extraction of magma from the crust and mantle. *Earth Planet. Sci. Lett.* **74**, 81–91.
- Melcher F., Sitnikova M., Graupner T., Martin N., Oberthür T., Henjes-Kunst F., Gäbler E., Gerdes A., Brätz H., Davis D. and Dewaele S. (2008) Fingerprinting of conflict minerals: columbite-tantalite (“coltan”) ores. *SGA News* **23**, 7–13.
- Michael P. J. (1983) Chemical differentiation of the Bishop Tuff and other high-silica magmas through crystallization processes. *Geology* **11**, 31–34.
- Miller C. F. and Mittlefehldt D. W. (1982) Depletion of light rare-earth elements in felsic magmas. *Geology* **10**, 129–133.
- Miller C. F. and Mittlefehldt D. W. (1984) Extreme fractionation in felsic magma chambers: a product of liquid-state diffusion or fractional crystallization? *Earth Planet. Sci. Lett.* **68**, 151–158.

- Möller P. and Muecke G. K. (1984) Significance of europium anomalies in silicate melts and crystal-melt equilibria: a re-evaluation. *Contrib. Mineral. Petrol.* **87**, 242–250.
- Monteyne-Poulaert G., Delwiche R. and Cahen L. (1962) Age de minéralisations pegmatitiques et filoniennes du Rwanda et du Burundi. *Ann. Soc. Geol. Belg.* **71**, 272–295.
- Mulja T., Williams-Jones A. E., Wood S. A. and Boily M. (1995) The rare-element-enriched monzogranite-pegmatite-quartz vein systems in the Preissac-Lacorne Batholith, Quebec. II. Geochemistry and petrogenesis. *Can. Mineral.* **33**, 817–833.
- Nash W. P. and Crecraft H. R. (1985) Partition coefficients for trace elements in silicic magmas. *Geochim. Cosmochim. Acta* **49**, 2309–2322.
- Neiva A. M. R. and Ramos J. M. F. (2011) Geochemistry of granitic aplite-pegmatite sills and petrogenetic links with granites, Guarda-Belmonte area, central Portugal. *Eur. J. Mineral.* **22**, 837–854.
- Olade M. A. (1980) Geochemical characteristics of tin-bearing and tin-barren granites, northern Nigeria. *Econ. Geol.* **75**, 71–82.
- Pan Y. (1997) Controls on the fractionation of isovalent trace elements in magmatic and aqueous systems: evidence from Y/Ho, Zr/Hf, and lanthanide tetrad effect—a discussion of the article by M. Bau (1996). *Contrib. Mineral. Petrol.* **128**, 405–408.
- Peeters L. (1956) Contribution à la géologie des terrains anciens du Ruanda-Urundi et du Kivu. *Ann. Has. Congo Belge. Geol.* **16**, 1–197.
- Philpotts J. A. and Schnetzler C. C. (1970) Phenocryst-matrix partition coefficients for K, Rb, Sr and Ba, with applications to anorthosite and basalt genesis. *Geochim. Cosmochim. Acta* **34**, 307–322.
- Pohl W. (1994) Metallogeny of the northeastern Kibara belt, Central Africa – recent perspectives. *Ore Geol. Rev.* **9**, 105–130.
- Pohl W. and Günther M. A. (1991) The origin of Kibaran (late Mid-Proterozoic) tin, tungsten and gold quartz vein deposits in Central Africa: a fluid inclusion study. *Miner. Deposita* **26**, 51–59.
- Pohl W., Biryabarema M. and Lehmann B. (2013) Early Neoproterozoic rare metal (Sn, Ta, W) and gold metallogeny of the Central Africa region: a review. *Appl. Earth Sci.* **122**, 66–82.
- Rayleigh J. W. S. (1896) Theoretical considerations respecting the separation of gases by diffusion and similar processes. *Philos. Mag.* **42**, 77–107.
- Roda-Robles E., Pesquera A., Velasco F. and Fontan F. (1999) The granitic pegmatites of the Fregeneda area (Salamanca, Spain); characteristics and petrogenesis. *Mineral. Mag.* **63**, 535–558.
- Roda-Robles E., Pesquera A., Gil-Crespo P. and Torres Ruiz J. (2012) From granite to highly evolved pegmatite: a case study of the Pinilla de Fermoselle granite-pegmatite system (Zamora, Spain). *Lithos* **153**, 192–207.
- Romer R. L. and Lehmann B. (1995) U-Pb columbite age of Neoproterozoic Ta-Nb mineralization in Burundi. *Econ. Geol.* **90**, 2303–2309.
- Selway J. B., Breaks F. W. and Tindle A. G. (2005) A review of rare-element (Li-Cs-Ta) Pegmatite exploration techniques for the Superior Province, Canada, and large worldwide tantalum deposits. *Explor. Min. Geol.* **14**, 1–30.
- Shaw D. M. (1968) A review of K-Rb fractionation trends by covariance analysis. *Geochim. Cosmochim. Acta* **32**, 573–601.
- Shearer C. K., Papike J. J. and Laul J. C. (1985) Chemistry of potassium feldspars from three zoned pegmatites, Black Hills, South Dakota: implications concerning pegmatite evolution. *Geochim. Cosmochim. Acta* **49**, 663–673.
- Shearer C., Papike J. J. and Jolliff B. L. (1987) Mineralogical and chemical evolution of a rare-element granite-pegmatite system: Harney Peak Granite, Black Hills, South Dakota. *Geochim. Cosmochim. Acta* **51**, 473–486.
- Shearer C., Papike J. J. and Jolliff B. L. (1992) Petrogenetic links among granites and pegmatites in the Harney Peak rare-element granite – pegmatite system, Black Hills, South Dakota. *Can. Mineral.* **30**, 785–810.
- Schnetzler C. C. and Philpotts J. A. (1970) Partition coefficients of rare-earth elements between igneous matrix material and rock-forming mineral phenocrysts; II. *Geochim. Cosmochim. Acta* **34**, 331–340.
- Simmons W. B. and Webber K. L. (2008) Pegmatite genesis: state of the art. *Eur. J. Mineral.* **20**, 421–438.
- Sirbescu M.-L. and Nabelek P. I. (2003) Crystallization conditions and evolution of magmatic fluids in the Harney Peak Granite and associated pegmatites, Black Hills, South Dakota—evidence from fluid inclusions. *Geochim. Cosmochim. Acta* **67**, 2443–2465.
- Štemprok M. (1987) Greisenization (a review). *Geol. Rundsch.* **76**, 169–175.
- Stilling A., Černý P. and Vanstone P. J. (2006) The Tanco pegmatite at Bernic Lake, Manitoba. XVI. Zonal and bulk compositions and their petrogenetic significance. *Can. Mineral.* **44**, 599–623.
- Suhr N. H. and Ingamells C. O. (1966) Solution technique for the analysis of silicates. *Anal. Chem.* **38**, 730–734.
- Tack L., Wingate M. T. D., De Waele B., Meert J., Belousova E., Griffin B., Tahon A. and Fernandez-Alonso M. (2010) The 1375 Ma ‘Kibaran event’ in Central Africa: prominent emplacement of bimodal magmatism under extensional regime. *Precambrian Res.* **180**, 63–84.
- Taylor S. R. (1965) The application of trace element data to problems in petrology. *Phys. Chem. Earth* **6**, 133–213.
- Theunissen K., Klerkx J., Melnikov A. and Mruma A. (1996) Mechanisms of inheritance of rift faulting in the western branch of the East African Rift, Tanzania. *Tectonics* **15**, 776–790.
- Thomas R. and Davidson D. (2012) Water in granite and pegmatite-forming melts. *Ore Geol. Rev.* **46**, 32–46.
- Thomas R., Davidson D. and Beurlen H. (2012) The competing models for the origin and internal evolution of granitic pegmatites in the light of melt and fluid inclusion research. *Miner. Petrol.* **106**, 55–73.
- Thomas R. and Davidson P. (2013) The missing link between granites and granitic pegmatites. *J. Geosci.* **58**, 183–200.
- Tindle A. G. and Breaks F. W. (2000) Columbite-tantalite mineral chemistry from rare-element granitic pegmatites: Separation Lake area, N.W. Ontario, Canada. *Miner. Petrol.* **70**, 165–198.
- Trueman D. L., Černý P. (1982) Exploration for rare-metal granitic pegmatites. In *Granitic Pegmatites in Science and Industry*. (ed. P. Černý). *Short Course Handbook*, vol. **8**. MAC. pp. 463–493.
- van Hinsberg V. J. (2011) Preliminary experimental data on trace-element partitioning between tourmaline and silicate melt. *Can. Mineral.* **49**, 153–163.
- Varlamoff N. (1954) Répartition des types de pegmatites autour de la partie nord-ouest du grand massif granitique de Nyanza. *Ann. Soc. Geol. Belg.* **78**, 1–21.
- Varlamoff N. (1956) *Carte Géologique Champs Pegmatitiques Gitarama Katumba*. RMCA, Tervuren, 1/50,000.
- Varlamoff N. (1963) Les phénomènes de greisenification, d'albitisation et de lépidolisation et leurs relations spatiales avec les granites et les pegmatites granitiques d'Afrique. *Ann. Soc. Geol. Belg.* **86**, 285–322.
- Varlamoff N. (1972) Central and West African rare-metal granitic pegmatites, related aplites, quartz veins and mineral deposits. *Miner. Deposita* **7**, 202–216.
- Webster J. D., Thomas R., Rhede D., Förster H. J. and Seltmann R. (1997) Melt inclusions in quartz from an evolved peralumi-

- nous pegmatite: geochemical evidence for strong tin enrichment in fluorine-rich and phosphorus-rich residual liquids. *Geochim. Cosmochim. Acta* **61**, 2589–2604.
- Yurimoto H., Duke E. F., Papike J. J. and Shearer C. K. (1990) Are discontinuous chondrite-normalized REE patterns in pegmatitic granite systems the results of monazite fractionation? *Geochim. Cosmochim. Acta* **54**, 2141–2145.
- Zhao J. X. and Cooper J. (1992) Fractionation of monazite in the development of V-shaped REE patterns in leucogranite systems: evidence from a muscovite leucogranite body in central Australia. *Lithos* **30**, 23–32.

Associate editor: Marc Norman